Phosphate $\delta^{13}C_{org}$ chemostratigraphy from the Gantour basin, Morocco: a proof of concept from the K–Pg transition to mid-Thanetian

Jérémie Aubineau[1*], Fleurice Parat[1], Anne-Catherine Pierson-Wickmann[2], Michel Séranne[1], Ernest Chi Fru[3], Radouan El Bamiki[4], Abdellatif Elghali[4], Otmane Raji[4], Manuel Muñoz[1], Clément Bonnet[1,5], Es-Said Jourani[4], Oussama Khadiri Yazami[6] & Jean-Louis Bodinier[1,4]

[1]Géosciences Montpellier, Université de Montpellier, CNRS UMR 5243, Montpellier, France

[2]Univ. Rennes, CNRS, Géosciences Rennes, UMR 6118, 35000 Rennes, France

[3]College of Physical and Engineering Sciences, School of Earth and Ocean Sciences, Centre for Geobiology and Geochemistry, Cardiff University, Cardiff CF10 3AT, Wales, UK

[4]Geology and Sustainable Mining Institute, Mohammed VI Polytechnic University, Ben Guerir 43150, Morocco

[5]ESRF, European Synchrotron Radiation Facility, Grenoble, France

[6]OCP, Strategic Development Department, Sustainability & Green Industrial Development, Khouribga 25000, Morocco

*corresponding author: jeremie.aubineau@umontpellier.fr

Abstract

The Late Cretaceous–early Paleogene interval is globally associated with transient to long-term changes in the stable carbon isotopic composition of marine carbonates ($\delta^{13}C_{carb}$). Based on biostratigraphic reconstruction, this critical period of Earth's history is thought to coincide with the deposition of world heritage Paleocene phosphate deposits (phosphorites) in northwestern Morocco. However, the detailed stratigraphy of the Gantour basin, one of the most important Moroccan phosphate deposits, has not yet been constrained. For instance, the former "Montian" Stage has been used to tentatively approximate the Danian, whereas the succeeding Selandian Stage remains to be identified. Here, we develop a detailed organic carbon isotopic ($\delta^{13}C_{org}$) curve from phosphorus-rich horizons of the western Gantour sedimentary sequence in an attempt to constrain their stratigraphic placement and depositional age model. Upsection, these strata host long-term negative and positive $\delta^{13}C_{org}$ trends that tend to correlate with global $\delta^{13}C_{carb}$ records of the Cretaceous–Paleogene and mid-Thanetian transitional boundaries. The data support the presence of Danian and Selandian rocks in the Gantour basin, which are succeeded by strata containing characteristic signatures of the well-known Cenozoic $\delta^{13}C$ maximum at 58–57.5 Ma (the Paleocene Carbon Isotope Maximum). Our results shift the previously proposed Cretaceous–Paleogene transition in the Gantour basin further down into the older sediment CM layer without interfering with recorded massive biological turnover in faunal diversity and abundance. Moreover, the refined stratigraphy suggests that the deposition of the Gantour phosphorites spanned ~8.5 Myr. Our results confirm the utility of $\delta^{13}C_{org}$ chemostratigraphy for dating and correlating phosphate-bearing deposits of the Tethyan province. They have important implications for deciphering Paleocene phosphogenesis, the co-evolution of associated vertebrate groups, and for prospecting phosphorus-rich mineral deposits.

Keywords: $\delta^{13}C_{org}$ chemostratigraphy, western Gantour basin, phosphorites, Paleocene, vertebrates.

1. Introduction

The Earth has undergone repeated climatic upheavals throughout its history. In particular, the dynamism of the climate during the early part of the Late Cretaceous was characterized by transient global temperature changes spanning tens of thousands of years, pCO_2 variability, and several millions of years of long-term deep-sea cooling and warming events (Barnet et al., 2018; Westerhold et al., 2020; Zachos et al., 2001, 2008).

For instance, the late Maastrichtian climate record reveals the rapid 2–3 °C warming of marine and terrestrial environments (Li and Keller, 1998a) ~150–300 kyr before the Cretaceous–Paleogene (K–Pg) boundary, which coincides with the onset of main pulse of Deccan volcanism covering most of western India (Barnet et al., 2018). The association of only a weak negative carbon isotope excursion (CIE) of ~0.5‰ with the emplacement of the Deccan Traps suggests that volcanic CO_2 emissions did not significantly perturb the global carbon cycle (Barnet et al., 2018). In contrast, the early Paleogene carbon isotope record of marine carbonates ($\delta^{13}C_{carb}$) is characterized by abrupt worldwide CIEs of ~1–3‰ (Kennett and Stott, 1991; Koch et al., 1992; Stap et al., 2010; Thomas and Zachos, 2000) that are thought to have resulted from the explosive release of metamorphic thermogenic methane into the ocean-atmosphere system (Dickens et al., 1997; Svensen et al., 2004). Such massive methane injections were likely inherited from the intrusion of voluminous mantle-derived melts into carbon-rich sedimentary deposits. These carbon additions triggered rapid (~10–20 kyr) hyperthermal global warming events such as the well-known Paleocene–Eocene Thermal Maximum (PETM), in which deep-sea temperatures rose dramatically to up to 5 °C (Westerhold et al., 2020; Zachos et al., 2001). Moreover, early Paleocene rocks contain evidence of similar events of smaller magnitude, including the Dan-C2 event and the Latest Danian Event (LDE) near the tops of Chron C29r and Chron C27n, respectively (Coccioni et al., 2010; Westerhold et al., 2011), although the former may not have impacted into the deep Pacific (Westerhold et al., 2011). Regardless of the spatial extents of the CIEs, the perturbations of the global carbon cycle resulting from these brief warming intervals are estimated to have lasted ~100–200 kyr (e.g., Coccioni et al., 2010; Kennett and Stott, 1991; Storme et al., 2012).

These transient climate and carbon cycle disturbances are superimposed on long-term benthic $\delta^{13}C_{carb}$ swings on the order of ±2.5‰ in the early Paleogene (Westerhold et al., 2020). Notably, a long-term decreasing trend in the benthic $\delta^{13}C_{carb}$

record is recognized from the latest Paleocene (~58 Ma) to the early Eocene, reaching its nadir during the Early Eocene Climatic Optimum (~51 Ma) (Zachos et al., 2001). This trend, coupled with a long-term decrease of $\delta^{18}O$ values in marine carbonates by ~1‰, is associated with some of the highest global temperatures and pCO_2 concentrations recorded during the Cenozoic (Westerhold et al., 2020; Zachos et al., 2001). Prior to the onset of this drastic warming episode, the mid to late Paleocene benthic $\delta^{13}C_{carb}$ record shows the most positive values of the Cenozoic; commonly referred to as the Paleocene Carbon Isotope Maximum (PCIM), it appears as a broad peak centered at ~58-57.5 Ma (Littler et al., 2014). Such positive $\delta^{13}C_{carb}$ values have been interpreted to result from a ~4 Myr global cooling event (Littler et al., 2014; Westerhold et al., 2020). Importantly, because of their ubiquity, the afore-mentioned negative CIEs and long-term rise and fall in $\delta^{13}C_{carb}$ compositions spanning the Late Cretaceous to early Paleogene have been used to correlate rock sequences worldwide (e.g., Aubry et al., 2007; Westerhold et al., 2020, 2011).

The global covariation of $\delta^{13}C_{carb}$ and sedimentary organic carbon isotopic ($\delta^{13}C_{org}$) values is assumed to reflect the common origin of both carbonate and organic matter from a contemporaneous dissolved inorganic carbon (DIC) reservoir with a consistent C isotopic composition (Bartley and Kah, 2004; Knoll et al., 1986; Korte and Kozur, 2010; Meyer et al., 2013; Storme et al., 2012), although meteoric alteration could simultaneously shift both $\delta^{13}C_{carb}$ and $\delta^{13}C_{org}$ values in a similar direction and magnitude (Oehlert and Swart, 2014). Classically, decoupled $\delta^{13}C_{carb}$ and $\delta^{13}C_{org}$ values may have been influenced by numerous factors, such as the mixing of two organic carbon pools, heterogeneous biological origins of total organic carbon (TOC), enhanced remineralization of marine organic carbon (Rothman et al., 2003), changes in atmospheric pCO_2 (Cramer and Saltzman, 2007; Young et al., 2008), and diagenetic alteration (Jiang et al., 2012). These considerations suggest that using $\delta^{13}C_{org}$ values alone may complicate global and regional stratigraphic correlations. Nevertheless, early Paleogene $\delta^{13}C_{org}$ trends from NW Morocco and other countries display features very similar to those of the calibrated reference $\delta^{13}C_{carb}$ curves (Noiret et al., 2016; Solé et al., 2019; Storme et al., 2012; Vandenberghe et al., 2012; Yans et al., 2014), highlighting their primary depositional synchroneity.

Here, we explored the organic carbon isotope ratios of phosphorites from the western Gantour basin (mining well 6258, Aubineau et al., 2022a) of NW Morocco (Figs. 1, 2) to reconstruct the $\delta^{13}C_{org}$ trend spanning the Late Cretaceous and early

Paleogene. Because phosphate sequences in NW Morocco may contain calcite, dolomite, and carbonate fluorapatite (CFA, $[Ca_{10-x-y}Na_xMg_y(PO_4)_{6-z}(CO_3)_z(F)_{0.4z}F_2]$; McClellan, 1980) in the same horizons (Aubineau et al., 2022a; Mouflih, 2015), we focused on the $\delta^{13}C_{org}$ record to avoid mixing inorganic carbon sources. Independent of lithofacies, we aimed to refine the poorly resolved stratigraphy of the western Gantour phosphate basin by focusing on organic carbon isotope chemostratigraphy because this approach has been successfully applied in the adjacent Ouled Abdoun phosphate basin (Yans et al., 2014). Our results provide a new stratigraphical framework for interbasin correlations of phosphorite horizons in NW Morocco, as well as highly resolved local biostratigraphic zones. Ultimately, our findings provide new age constraints on the world's largest phosphate accumulation.

2. Geological background

2.1. General information

Phosphorus-bearing rocks of NW Morocco span the K–Pg boundary and extend into the Eocene (Hollard et al., 1985; Lucas and Prévôt-Lucas, 1995; OCP, 1989). Notably, the Ouled Abdoun and Gantour basins (western Meseta) are two of the four most important sedimentary phosphorus-rich basins in Morocco (Fig. 1; El Bamiki et al., 2021). Structurally, this part of NW Morocco formed from thermal subsidence during the opening of the central Atlantic Ocean during the Late Triassic to Early Jurassic (Michard et al., 2008), which enabled the accumulation of Mesozoic marine sedimentary successions along the eastern passive margin of the central Atlantic Ocean. Thereafter, eustacy mainly controlled the sedimentation dynamics during the Late Cretaceous to early Paleogene. Then, because of rising sea levels, flooding of large parts of western Morocco resulted in the landward migration of the phosphogenic window and the subsequent deposition of sedimentary phosphates and shallow marine carbonates (El Bamiki et al., 2020; Michard et al., 2008). In addition to the biological liberation of organic-bound phosphorus into porewaters, localized storm and bottom water currents have repeatedly winnowed the primary phosphate layers (<10 wt.% P_2O_5), contributing to the formation of phosphorites (>18 wt.% P_2O_5) (El Bamiki et al., 2020; Glenn et al., 1994; Pufahl and Groat, 2017; Ruttenberg, 2003).

The Gantour basin is extensively exploited in large industrial quarries by the "Office Chérifien des Phosphates" (OCP). Phosphorus-rich horizons were excavated in successive bearings, from top to bottom, which promoted Arambourg's (1935, 1952) pioneering biostratigraphic studies. The Upper Cretaceous pre-phosphate series of the Gantour basal sediments is mainly characterized by dolomitized marls and sandstones (Boujo, 1976). The overlying phosphate series comprises Maastrichtian marls, limestones, and phosphatic sands interbedded with thin phosphorite layers (Fig. 2), in turn overlain by yellowish clays that probably constitute a marker layer within the Gantour basin (Cappetta et al., 2014; Noubhani and Cappetta, 1997; OCP, 1989). Thick phosphorite layers overlying the yellow clays span the late Maastrichtian to Ypresian and were deposited in a marl-dominated environment. Following the mining terminology (in French), the “C2S”, “C2M”, and “C2I” levels (Fig. 2) are “Couche 2 supérieure”, “Couche 2 médiane”, “Couche 2 inférieure”, respectively, or “Level 2 upper”, “Level 2 middle”, and “Level 2 lower”, respectively (Cappetta et al., 2014). For clarity, we abbreviate all phosphorite levels. Furthermore, the “Sillon X” or “SX” level might correspond to the uppermost Maastrichtian phosphorites of the Gantour sequence, based on the mining nomenclature (Fig. 2; Bardet et al., 2017; Boujo, 1976; Noubhani and Cappetta, 1997; OCP, 1989). Considering the low abundances of clay materials associated with many coated phosphate grains and broken bone fragments in the Gantour phosphorites, a high-energy hydrodynamic regime controlled by repeated hydrodynamic winnowing and reworking must have prevailed in the depositional sites (Aubineau et al., 2022a). Finally, Lutetian *Thersitea* dolomitic limestones regionally cap the NW Moroccan phosphate series, although they are locally eroded in the Gantour basin (Boujo, 1976; El Bamiki et al., 2021; Salvan, 1955).

2.2. The Moroccan phosphate fauna

The biostratigraphy of the NW Moroccan phosphate series primarily relies on fossiliferous selachians (sharks and rays) and marine reptiles (Fig. 2) (Arambourg, 1952, 1935; Cappetta et al., 2014; Lebrun, 2020; Noubhani and Cappetta, 1997, and references therein). More than 50% of Maastrichtian vertebrate species in Morocco also occur in many well-calibrated sections worldwide (Cappetta et al., 2014; Noubhani and Cappetta, 1997). However, the Paleocene faunal content is sparse in the Moroccan phosphate series, and many marine species are geographically restricted, hindering biostratigraphic correlations with other provinces. Nonetheless, seven shark species in the “C0–C1” Gantour level (*Palaeogaleus brivesi*, *Squatina prima, Ginglymostoma subafricanum, Carcharias tingitana, Odontaspis speyeri, Striatolamia whitei,* and *Prosopodon assafai*) are correlated with Danian rocks in Europe, Africa, and North America, although the base of the Danian Stage has yet to be constrained (Fig. 2; Noubhani and Cappetta, 1997). The discovery of selachian fossils of Ypresian age in Morocco is supported by faunal similarities with fossiliferous deposits in Europe and the USA (Fig. 2; Noubhani and Cappetta, 1997).

More specifically, the vertebrate faunas of Gantour are essentially Maastrichtian in age, whereas the Ouled Abdoun fossils are typical of the early Paleogene (Arambourg, 1952, 1935; Bardet et al., 2017; Cappetta et al., 2014; Noubhani and Cappetta, 1997). Indeed, the Ouled Abdoun basin has yielded the richest faunas and best-preserved tetrapod fossils (Bardet et al., 2017). Notably, those sediments appear more attractive for paleontological investigations because they have yielded the most primitive elephants (Gheerbrant, 2009; Gheerbrant et al., 1998). In contrast, remains of terrestrial mammals have never been described in the Gantour basin (Bardet et al., 2017). A comprehensive review of vertebrate faunas in the NW Moroccan phosphate basins reveals the preservation of more than 330 species of selachians, bony fishes (*i.e.*, actinopterygians), reptiles (including birds), and mammals (Bardet et al., 2017). Other biostratigraphic data derive from studies of pollens in extremely low abundance (Ollivier-Pierre, 1982), dinoflagellates (Rauscher and Doubinger, 1982), and foraminifers and mollusks (Salvan, 1955). Nonetheless, these have proven less useful than selachian assemblages for biostratigraphic correlations.

2.3. Stratigraphy of the Gantour phosphate basin

The NW Moroccan phosphate series hosts abundant vertebrate species spanning a period of nearly 25 Myr from the Maastrichtian to the Lutetian (Bardet et al., 2017; Lebrun, 2020; Noubhani and Cappetta, 1997). Biostratigraphic correlations with well-dated faunal assemblages from other African, North American, and European provinces emerged across the Maastrichtian, Ypresian, and Lutetian (Arambourg, 1952; Noubhani and Cappetta, 1997). However, the Paleocene stratigraphy specific to the Gantour phosphate rocks needs to be better resolved (Fig. 2; OCP, 1989). The current Paleocene stratigraphy presented in Figure 2 and established by the OCP group in the 1980s is highly questionable due to the absence of robust evidence constraining their assignments of stage boundaries. To our knowledge, however, their work remains the only English reference locating the western Gantour phosphate horizons. This stratigraphy likely integrated Selachian biozonations described by Arambourg1952, 1935). Arambourg was suspicious about the presence of the Danian

Stage in the NW Moroccan phosphate basins, and thus used the terms “Montian” or “Dano-Montian” to describe Lower Paleocene rocks (Arambourg, 1952, 1935; Cappetta, 1987). Dewalque (1868) introduced the “Montian” Stage at the base of the Paleogene (named after Mons, Belgium) in the nineteenth century, a stage supposedly younger than the Danian (Vandenberghe et al., 2012). Nonetheless, the “Montian” Stage lost its significance because it is related only to a local facies and is based on a compromising stratotype that is not suitable for stratigraphic correlations (Vandenberghe et al., 2012). Later, the term “Danian” was used to define the early Paleocene portion of the NW Moroccan phosphate series, though without ascertaining its synchronism with well-calibrated Danian rocks in other areas (Noubhani and Cappetta, 1997). Furthermore, despite the absence of a sedimentary hiatus in the Maastrichtian–Lutetian phosphate interval (Arambourg, 1952; Boujo, 1976; Noubhani, 2010), the Selandian Stage has never been paleontologically reported in the Gantour basin (Noubhani, 2010). In fact, the threefold subdivision of the Paleocene was not officially recognized until 1989 (Vandenberghe et al., 2012), well after Arambourg established his biostratigraphy between 1935 and 1952. Thus, the former early Thanetian Stage is implied to include the current Selandian Stage. Collectively, the Paleocene stratigraphy of the Gantour phosphate basin remains unexplored and unconstrained, making it considerably difficult to unravel the impact of lateral facies changes on biostratigraphy.

Refining the stratigraphy of the Moroccan phosphate series is therefore crucial because previous biostratigraphic age determinations have now come into question, as recently demonstrated by new age constraints (El Bamiki et al., 2020; Yans et al., 2014). Notably, calcareous nannofossils in the Moroccan High Atlas (MHA) phosphate series have yielded ages several million years older than previously established (El Bamiki et al., 2020). In the Ouled Abdoun area, $\delta^{13}C_{org}$ chemostratigraphy revealed a possible hiatus in the upper Thanetian and did not support the Lutetian Stage in the phosphate series (Yans et al., 2014). Such age disparities are likely caused by reworking (Gheerbrant et al., 2003), the diachronous nature of facies in the Moroccan phosphate-bearing deposits (Boujo, 1976; El Bamiki et al., 2020), and personal research interests focusing on species’ evolutionary aspects rather than the stratigraphic framework (Lebrun, 2020). Kocsis et al. (2014) performed chemostratigraphic studies based on $\delta^{18}O_{PO4}$ and $\delta^{13}C_{CO3}$ values of biogenic apatite from the eastern Gantour phosphate series. However, their trends were of relatively low resolution and had significant uncertainties. Moreover, stratigraphic correlations have been proposed between the Gantour and Ouled Abdoun basins likely solely based on biostratigraphy (Bardet et al., 2017), and no details were provided to explain how these correlations were constructed. Notably, Noubhani and Cappetta (1997) were not convinced of the correlations for the bases of the Maastrichtian, Danian, Thanetian, and Ypresian stages between Morocco and Europe. In light of these considerations, new approaches independent of lithological investigations are needed to further characterize the Late Cretaceous to early Paleogene interval in NW Moroccan phosphate-bearing rocks.

3. Methodology

OCP geologists collected 23 samples corresponding to different phosphorus-rich horizons from 0.15–0.80-m-thick intervals in mining well 6258, in the western Gantour basin (Fig. 1b, Table 1). In addition, although biostratigraphic studies were never performed in this specific section, OCP geologists performed step-by-step stratigraphic correlations of P-rich horizons thanks to hundreds of mining exploration wells (Mouflih, 2015). However, the thickness of the sampled intervals and the lenticular appearances of some phosphate-bearing levels may have generated uncertainties in their data interpretation.

Petrographic, bulk mineral, and *in-situ* geochemical examinations of selected Gantour samples were recently performed (Aubineau et al., 2022a). We now provide the mineralogical compositions of all Gantour bulk-powder samples as obtained by X-ray diffraction (XRD). Detailed XRD analytical and data treatment procedures are provided in Aubineau et al. (2022a). Semi-quantitative bulk mineral proportions were determined by Rietveld refinement of acquired XRD patterns using the Profex 4.3.1 interface within the program BGMN (Döebelin and Kleeberg, 2015).

Whole-rock major element concentrations were measured by inductively coupled plasma optical emission spectrometry at Service d'Analyse des Roches et Minéraux (SARM) of the Centre de Recherches Pétrographiques et Géochimiques, Nancy, France. Samples were prepared according to the protocol of Carignan et al. (2001), which is summarized here. Whole-rock powders were dissolved with nitric acid and fused with 900 mg ultra-pure lithium metaborate at 980 °C to form a glass substrate used for analysis. Sulfur contents were determined using a C/S elemental analyzer, whereas F and Cl were measured by wet precipitation ferrithiocyanate spectrophotometry on a Varian Cary 50 218 spectrophotometer at SARM. Geochemical data, uncertainties, and detection limits are presented in Table S1.

For organic C isotopic analysis and determination of TOC contents, more than 200 mg of whole-rock powders were initially treated with 6 N HCl for one hour at 70 °C to remove carbonates and carbonate fluorapatite. Residues were then rinsed repeatedly in deionized water and subsequently dried in a clean hood. Aliquots of decarbonated samples were weighed into tin cups, and their $\delta^{13}C_{org}$ values and TOC contents measured with an elemental analyzer (EA, Isolink - Thermo Scientific, Bremen, Germany) coupled to a Delta V isotope ratio mass spectrometer (Thermo Scientific) at the PISTE Platform (OSUR, Rennes, France). Sample combustion was conducted at 1020 °C in the presence of ~10 mL O_2. Isotopic measurements were calibrated against the international reference USGS-24, with internal standards including glutamic acid, urea, and humic acid supplied by Aldrich. Analytical uncertainty was estimated to be lower than 0.1‰. Carbon isotopic data are reported in δ-notation relative to Vienna Peedee belemnite, and TOC contents extrapolated from the volume of evolved CO_2.

4. Results

Inferred mineralogical assemblages mainly included calcite, dolomite, CFA, and quartz throughout the section (Fig. 3a, Table S2), with lesser amounts of clay minerals and titanium oxides. Smectite is the dominant phyllosilicate in the Gantour basin (Aubineau et al., 2022a). Binary plots between TOC/Si and selected major elements were used to decipher whether the delivery of organic matter to the western Gantour basin was controlled mainly by the detrital flux or marine productivity. TOC has been normalized to Si to remove the sediment dilution effect (Fig. 3b). Using Al and Ti as reliable detrital tracers (Tribovillard et al., 2006), TOC/Si was found to show moderate negative correlations with Al_2O_3 ($R^2 = 0.37$, $p < 0.001$) and TiO_2 ($R^2 = 0.32$, $p < 0.003$). However, P_2O_5 displayed a moderate positive correlation with TOC/Si ($R^2 = 0.33$, $p < 0.002$), but no correlation with Al_2O_3 ($R^2 = 0.04$, $p < 0.34$).

The 23 phosphorite samples studied along this stratigraphic interval of the western Gantour basin had $\delta^{13}C_{org}$ values in the range −26.7‰ to −28.5‰, similar to phosphorites from Ouled Abdoun (Yans et al., 2014), and contained 0.3–1.5 wt.% TOC (Fig. 4; Table 1). $\delta^{13}C_{org}$ values showed a weak negative correlation with TOC (Fig. 4; $R^2 = 0.27$, $p < 0.008$). Moving upsection from the base of the lowest phosphorite level,

$\delta^{13}C_{org}$ values first show a brief and slight increase by 0.14‰ within the "C2M" level (35.43–34.38 m depth, Fig. 4). This is then followed by a progressive upward decrease from −27.0‰ at 33.93 m depth ("C2M" level) to −28.5‰ at 27.13 m depth (DSP1 level) before increasing again to −26.7‰ at 16.15 m depth (SFA1S level). The section is capped by mostly invariant $\delta^{13}C_{org}$ values to 12.7 m depth (NAB level); these relatively constant $\delta^{13}C_{org}$ values are distinct from the dramatic fluctuations observed in the underlying lithologies.

5. Discussion

5.1. Origin of organic matter

A central issue of $\delta^{13}C_{org}$ chemostratigraphy is the mixing of organic matter from terrestrial and marine sources with potentially variable carbon isotopic compositions (Bodin et al., 2023; Bomou et al., 2021; Sluijs and Dickens, 2012). For instance, the $\delta^{13}C$ values of terrestrial C3 plants were a few per mil higher than those of contemporaneous marine organic carbon during the Paleocene and Eocene (Domingo et al., 2009). If the organic matter in question is of continental origin, TOC tends to covary in part with Al- and Ti-containing detrital materials (Bodin et al., 2023; Bomou et al., 2021). Although preserved in low abundances, smectites, being Al-bearing swelling phyllosilicates, are the only Al-rich mineral phase in the western Gantour phosphorites. Because Al substitution in apatite group minerals is unlikely (Nathan, 1984; Pan and Fleet, 2002) and smectite initially derives from continental weathering (Meunier, 2005), it is appropriate that we use Al as a tracer of detrital sources.

The absence of any meaningful positive covariation between TOC/Si and Al_2O_3 or TiO_2 contents in our phosphorites implies that it is unlikely that the organic matter supply to the basin was linked to riverine sources. In contrast, organic carbon was closely tied to marine productivity, as demonstrated by the moderate correlation between TOC/Si and P_2O_5 concentrations. Moroccan CFA minerals formed immediately below the water-sediment interface, under the influence of coastal upwelling (Pufahl and Groat, 2017). In such environments, large fluxes of sinking organic-bound phosphorus fuel the precipitation of sedimentary CFA and microbially mediated organic matter remineralization promotes the supersaturation of dissolved inorganic P in sediment porewaters (Ruttenberg, 2003). Moreover, the lack of correlation between Al_2O_3 and P_2O_5 in the studied phosphorites suggests that the delivery of phosphate and associated smectite particles from the land to the oceans was limited. Hence, it is reasonable to assume that the western Gantour basin hosts marine organic carbon, and that organic matter was the main source of P enrichment in the sediments during phosphogenesis.

Although the Ouled Abdoun phosphogenic basin extended landwards relative to western Gantour and is characterized by the occurrence of continental mammal fossils (Bardet et al., 2017), the contribution of terrestrial organic carbon there is considered negligible (Kocsis et al., 2014; Yans et al., 2014). This observation provides further support for the predominantly marine origin of organic matter in the western Gantour basin.

5.2. Diagenetic and weathering considerations

The mobilization of cations and anions and the decarbonation of CFA during post-depositional alteration may strongly affect CFA composition and, eventually, the formation of fluorapatite (McClellan and Van Kauwenbergh, 1991). For example, these alternative processes result in a systematic loss of sedimentary CO_3^{2-}. In contrast, the western Gantour CFA grains contain 7.4 ± 0.7 wt.% CO_3^{2-} on average (1σ, n = 5) in their crystal lattices (Aubineau et al., 2022a), comparable to the 5–8 wt.% CO_3^{2-} in unaltered CFA in equilibrium with seawater (Nathan, 1984). This evidence suggests that the Gantour CFA minerals experienced little to no post-depositional alteration. Indeed, the presence of smectite and the absence of illite/smectite mixed-layer minerals in the studied samples (Aubineau et al., 2022a) indicate limited mineralogical diagenetic transformations by heating (Środoń and Eberl, 1984; Velde et al., 1986). This can be easily explained by the overall low burial rates of the Gantour sediments. For example, in the western Meseta, Charton et al. (2021) calculated a maximum burial rate of 50 m/Myr. Sediment deposition continued for 25 Myr after the formation of the first phosphorite horizon (the phosphate series was capped by Lutetian *Thersitea* dolomitic limestones), implying that the Gantour rocks were not buried to depths exceeding 1,300 m. In the Paleocene, the western Meseta corresponded to the High Atlas rift flanks (Michard et al., 2008). The flanks of modern rift systems display geothermal gradients of 25–30 °C/km (Van der Beek et al., 1998). Based on these considerations, thermal alteration in the Gantour phosphate series was probably limited because the maximum temperature experienced during burial was <40 °C.

Thermal diagenesis can affect the primary carbon isotopic composition of organic carbon. For instance, the diagenetic transformation of organic matter during microbial respiration and thermal breakdown decreases sedimentary TOC content, while the loss of isotopically light ^{12}C enriches the residual organic matter in isotopically heavy ^{13}C (Hayes et al.,1983). Diagenetic transformations therefore generate a strong correlation between $\delta^{13}C_{org}$ and TOC that is not observed in our samples. Considering this alongside the absence of metamorphism in these sediments, we conclude that thermal alteration and weathering did not exert a significant impact on the primary $\delta^{13}C_{org}$ signature. Therefore, because the studied sediments were not subjected to episodes of destructive alteration, coupled primary variations of $\delta^{13}C_{carb}$ and $\delta^{13}C_{org}$ should be preserved.

5.3. $\delta^{13}C_{org}$ chemostratigraphy: a new age calibration for the Gantour basin

Sedimentation rates <20 m/Myr usually characterize upwelling phosphogenic zones along modern continental shelves (Filippelli, 1997), resulting in the formation of condensed phosphate sequences. Indeed, phosphorites accumulated on the North African shelf during the Late Cretaceous and Paleogene formed from active coastal upwellings (Pufahl and Groat, 2017), e.g., with extremely low sedimentation rates of ~2 m/Myr inferred in the Ouled Abdoun basin (Yans et al., 2014). In addition, depositional hiatuses during the upper Thanetian may have contributed to the highly condensed character of the section (Gheerbrant et al., 2003; Yans et al., 2014). Moreover, the phosphate-bearing series of the western Gantour and Ouled Abdoun basins were deposited contemporaneously in the same paleogeographic province (El Bamiki et al., 2021). It is thus rational to assume that an extremely low sedimentation rate also controlled deposition of the ~25-m-thick phosphorite interval in the western Gantour basin.

The specific Maastrichtian, Danian, and Ypresian vertebrate faunas present in the western Gantour phosphate series (Fig. 2; Arambourg, 1952; Cappetta et al., 2014; Noubhani and Cappetta, 1997) enabled the initial stratigraphic placement of our $\delta^{13}C_{org}$ curve with respect to the global $\delta^{13}C_{carb}$ curve. In this context, long-term isotopic trends can be elucidated more confidently than short-term abrupt trends or transient CIEs. Indeed, synchronous $\delta^{13}C$ records in carbonates and organic-bearing strata during the Paleogene have promoted global correlations (Noiret et al., 2016; Solé et al., 2019; Storme et al., 2012; Yans et al., 2014). Therefore, in this subsection, we compare the $\delta^{13}C_{org}$ trend in western Gantour phosphorites to the Cenozoic global reference benthic carbon isotope dataset (Westerhold et al., 2020) and the established $\delta^{13}C_{org}$ curve for the Ouled Abdoun phosphate basin (Yans et al., 2014) with the aim of better refining the Paleocene stratigraphy of the western Gantour phosphate series. A striking feature of the global $\delta^{13}C_{carb}$ trend during the Paleogene is that the heaviest carbon isotopic composition is recorded in the mid-Thanetian (Westerhold et al., 2020), whereas sediments deposited during the late Maastrichtian do not tend to show such high $\delta^{13}C_{carb}$ values (Li and Keller, 1998a, 1998b). Considering these temporal and depositional constraints, our $\delta^{13}C_{org}$ pattern mimics the long-term Paleocene $\delta^{13}C_{carb}$ trends (Fig. 5). However, based on the presence of Danian fossils in the "C0–C1" level (Fig. 2), most of the $\delta^{13}C_{org}$ profiles at Gantour cannot be correlated with the Ouled Abdoun isotopic curve (Fig. 5). The highest $\delta^{13}C_{org}$ values observed in the mid-Thanetian are followed by a long-term negative $\delta^{13}C_{org}$ excursion down to the lowest $\delta^{13}C_{org}$ values measured in the Eocene, then by sediments with a unique long-term positive $\delta^{13}C_{org}$ trend (Yans et al., 2014). Importantly, the $\delta^{13}C_{org}$ values of the Ypresian are not as high as those of the Paleocene Carbon Isotope Maximum. This discrepancy provides further information guiding the placement of the significant $\delta^{13}C_{org}$ variations observed at Gantour within the Paleocene $\delta^{13}C_{org}$ record.

5.3.1. Latest Danian to mid-Thanetian

We have organized our discussion backward through time because of a best constraint for younger rocks. The positive $\delta^{13}C_{org}$ trend, increasing by 1.8‰, upward from the "DSP1" level to the "SFA1S" level in the western Gantour basin is quite similar to the ~1.4‰ increase in the 1-Myr smoothed benthic $\delta^{13}C_{carb}$ record from middle to late Paleocene marine sedimentary facies (Fig. 5). The reference isotopic record for this interval is characterized by a gradual long-term shift toward the highest $\delta^{13}C$ values ever observed during the PCIM. Specifically, the inflection point of the $\delta^{13}C_{carb}$ trend prior to the maximum $\delta^{13}C_{carb}$ composition occurs very close to the boundary between Chrons C27n and C26r in the latest Danian (Westerhold et al., 2020). This inflection point is suggested to occur in the "DSP1" level associated with the lowest $\delta^{13}C_{org}$ value observed in the studied interval (Fig. 4). Alternatively, the "DSP1" level might be correlated with sediments between the upper part of Chron C29n and C27n/C26r boundary because of the monotonic upward decrease in $\delta^{13}C_{carb}$ values within this interval. An extremely low sedimentation rate or depositional hiatus in the NP2, NP3, and NP4 Zones, although never identified (Arambourg, 1952; Boujo, 1976; Noubhani, 2010), would support such a correlation. Because this latter proposition is less parsimonious, we prefer the former.

The base of the Selandian Stage appears at the top of the lower third of Chron C26r (Vandenberghe et al., 2012). In addition, basal Selandian sediments are generally correlated with the radiation of important calcareous nannofossil species affiliated with NP5 biozones (Schmitz et al., 2011). In the western Gantour phosphate series, the Danian–Selandian boundary is most likely between the “DSP1” and “DSP2” levels, although its exact stratigraphic position remains uncertain because no additional data are available. However, benthic $\delta^{13}C_{carb}$ records progressively increase from the Selandian to the early Thanetian (Westerhold et al., 2020, 2011), in agreement with our observed $\delta^{13}C_{org}$ trend. Although there is no $\delta^{13}C_{carb}$ anomaly associated with the base of the Thanetian in the deep-sea marine record (Schmitz et al., 2011; Vandenberghe et al., 2012; Westerhold et al., 2011, 2020), the highest $\delta^{13}C_{carb}$ values of the PCIM are recognized in the upper part of Chron C25r (Westerhold et al., 2020), at ~58-57.5 Ma in the mid-Thanetian. The “SFA1” level in the western Gantour basin hosts the most positive $\delta^{13}C_{org}$ values, although the overlying “NAB” level displays comparable carbon isotopic ratios (Fig. 4). In the Ouled Abdoun phosphate series, “Bed IIa” or the “C2a” level—distinct from the “C2” level at Gantour—record increasing $\delta^{13}C_{org}$ values reaching as high as −25.9‰, which was previously dated as early Thanetian and belonging to Chron C25r (Fig. 5; Yans et al., 2014). Our recognition of a long-term positive $\delta^{13}C$ trend until these highest $\delta^{13}C$ values, here related to the PCIM, implies that the uppermost phosphorite horizons of the western Gantour basin are precisely associated with the early to middle Thanetian and to Chron C25r (Fig. 5). The interval between the Chron C27n/C26r boundary and the upper part of Chron C25r thus accounts for a total duration of up to ~4.5 Myr, and thus an overall low sedimentation rate of 2–3 m/Myr in the western Gantour phosphorites. Finally, we speculate that the marls and phosphatic calcareous sands overlying the phosphorite-rich interval belong to the upper Thanetian and Ypresian, but this remains poorly constrained.

5.3.2. K–Pg transition to latest Danian

The Danian Stage is marked by a long-term decrease of deep-sea $\delta^{13}C$ values by >0.8‰ over ~4 Myr from the lower part of Chron C29r to Chrons C27n–C26r (Westerhold et al., 2020), as well as negative CIE of 0.6‰ near the top of Chron C27n.

The western Gantour $\delta^{13}C_{org}$ values recorded between the upper part of the "C2M" level and the "DSP1" level show a similar long-term upward decrease by 1.5‰ (Fig. 5). This $\delta^{13}C_{org}$ drift would have started at the K–Pg transition at ~66 Ma and extended upwards into the minimum values of the latest Danian, at ~62 Ma (Fig. 5). Abrupt spikes of the deep-sea $\delta^{13}C$ values at ~66 and ~62 Ma may explain the larger magnitude of the carbon isotopic fluctuations observed in the western Gantour phosphorites (1.5‰) compared to the gradual long-term $\delta^{13}C_{carb}$ shift (0.8‰). Despite the presence of a ~1.5-Myr decrease of benthic $\delta^{13}C_{carb}$ values across Chron C30n in the late Maastrichtian (Li and Keller, 1998a, 1998b), the absence of any apparent geological hiatus in the Gantour basin near the K–Pg transition (Arambourg, 1952; Boujo, 1976; Noubhani, 2010) hints that phosphorites from the lower part of the studied section do not belong to the Maastrichtian. With this in mind, our data imply that the base of the Cenozoic Era is deeper in the section, as demonstrated by the sharp inflection in our $\delta^{13}C_{org}$ curve (Fig. 4), which we correlate to that in the established benthic $\delta^{13}C_{carb}$ reference (Fig. 5). Overall, this suggests that the western Gantour phosphorites between the upper part of the "C2M" level and the "DSP1" level were deposited within ~4 Myr under low sedimentation rates of perhaps <2 m/Myr. Consequently, we propose that the "SX" level no longer be used as a marker of the K–Pg boundary at Gantour because our data show it to be a few million years younger.

5.3.3. Latest Maastrichtian

The lowermost phosphorus-rich level, represented by the lower part of the "C2M" level, likely coincides with the latest Maastrichtian (Fig. 4). The increasing $\delta^{13}C_{org}$ trend at that level may correspond to the global cooling event recorded in the uppermost Maastrichtian rocks, as supported by the concomitant increase and decrease of $\delta^{13}C_{carb}$ and $\delta^{18}O_{carb}$ values, respectively (Thibault et al., 2016; Zachos et al., 1989). Nonetheless, further examination of the $\delta^{13}C_{org}$ records of the lower phosphate series in the western Gantour basin is required to confidently establish this latter proposition. In light of these and above considerations, our data reveal that the western Gantour basin encompasses a ~8.5 Myr window spanning the K–Pg transition to the mid-Thanetian, including the lower and upper parts of Chrons C29r and 25r, respectively.

5.4. Insights for stratigraphic correlations of Moroccan phosphate deposits

Our new age constraints suggest that the upper phosphate series of the western Gantour basin is slightly older than the upper phosphate successions of the Ouled Abdoun basin (whose age constraints rely on chemostratigraphy and vertebrate faunas; Gheerbrant, 2009; Gheerbrant et al., 2003; Yans et al., 2014). However, in both basins, upwards positive $\delta^{13}C_{org}$ trends from the Selandian to mid-Thanetian allows for interbasinal stratigraphic correlations of phosphorite horizons, and for the identification of a homogenous basin-scale $\delta^{13}C_{org}$ distribution. Considering the highest $\delta^{13}C_{org}$ values related to the PCIM at ~58-57.5 Ma, the western Gantour "SFA1S" level correlates with the top of the "C2a" level in the Ouled Abdoun basin (Fig. 6a). The latter also connects with phosphorite intervals containing the "SFA3I", "SFA3S", "SFA2M", "SFA2S", and "SFA1S" lithologies. However, additional $\delta^{13}C_{org}$ data are required to unambiguously validate this correlation. As previously demonstrated in the MHA phosphate series, complexities of U-Pb CFA dating indicate discrepancies between sediment depositional ages and the time of lithification, compromising stratigraphic correlations using this method (Aubineau et al., 2022b). In contrast, biostratigraphic data from calcareous nannofossils seem more robust (El Bamiki et al., 2020) and have facilitated the stratigraphic resolution of the exploited phosphate facies. Indeed, we correlate the western Gantour "SFA1S" and Ouled Abdoun "C2a" phosphorite levels of mid-Thanetian age with the MHA marly interval that underlies the carbonates of late Thanetian age (Fig. 6a).

Our new $\delta^{13}C_{org}$ dataset, together with the prior $\delta^{13}C_{org}$ curve of Yans et al. (2014), enable the extraction of new important information regarding the stratigraphical framework of as-yet uncalibrated sections. Assuming that intrabasinal connections of mining levels are unambiguous between the western and eastern Gantour basins, we here propose correlations between the well-calibrated Bouchane section and the poorly constrained eastern Gantour sections to allocate to them their appropriate stratigraphic ages (Fig. 6b). In this regard, we correlate the K–Pg boundary to somewhere within the eastern Gantour "C2" level, although, to our knowledge, the lack of subdivisions in this level does not allow us to be more specific. Moreover, correlations of phosphorite levels between calibrated phosphate series and other studied Ouled Abdoun phosphate sections are not straightforward (Fig. 6b). While the Ouled Abdoun "C2a" level is a correlative horizon as mentioned above, further $\delta^{13}C_{org}$ correlations for these strata remain to be determined. Nevertheless, the coupling of the unique $\delta^{13}C_{org}$ trends of the NW Moroccan phosphorite facies to well-established global reference $\delta^{13}C_{carb}$ records hint that $\delta^{13}C_{org}$ chemostratigraphy is an appropriate correlation tool for these phosphate-bearing sequences.

5.5. Implications for dating the Gantour vertebrate faunas

Improving our knowledge of the biostratigraphy of the Moroccan phosphorites is of paramount importance due to their faunal renewal capacity during the Maastrichtian–Lutetian interval (Bardet et al., 2017). Although several attempts have been made to establish correlations between the NW Moroccan phosphorite horizons (Arambourg, 1952; Bardet et al., 2017; Kocsis et al., 2014), we prefer not to consider them here because of the obvious lack of sequence stratigraphic framework and clear allocation approaches (see Section 2.3). Our new stratigraphic correlations with respect to the calibrated $\delta^{13}C$ curves indicate that the K–Pg transition is most likely in the upper part of the Gantour "C2M" level.

Based on data acquired from thousands of isolated fossil teeth collected over many decades, Cappetta et al. (2014) provided a complete faunal list of Maastrichtian marine vertebrates in the eastern Gantour basin. Marine reptiles, including elasmosaurid plesiosaurs, mosasaurid *species*, and pachyvaranid squamates, and several selachian families such as Anacoracidae, Hypsobatidae, Pseudocoracidae, Sclerorhynchidae, and Rhombodontidae, abruptly disappeared during the K–Pg extinction event (Bardet, 2012; Cappetta, 1987; Cappetta et al., 2014; Lebrun, 2020). However, the fossilized remains of these marine reptiles and selachians in the eastern Gantour basin have been found to be abundant in the "C2" level, although their stratigraphic subdivisions and sampling positions have never been properly reported (Cappetta et al., 2014; Noubhani and Cappetta, 1997). In addition, Cappetta et al. (2014) observed that mosasaurid and pachyvaranid squamates were preserved throughout the Maastrichtian succession, except in two horizons, one of which being the "SX" level. This latter phosphorite horizon is sometimes characterized by a mixture of Maastrichtian and Danian vertebrate faunas (Cappetta et al., 2014), suggesting either its diachronous nature or a sampling bias possibly caused by mining exploitation. Regardless of these faunal uncertainties, the pervasive absence of some key marine reptiles and selachians that went extinct during the K–Pg event is best explained if the "SX" level is considered to be Danian rather than late Maastrichtian in age. Although the above vertebrate groups were abundant and diverse during the latest Cretaceous (Cappetta et al., 2014), their last occurrences probably coincided with the deposition of the "C2M" phosphorite. Future exhaustive and integrated litho-biostratigraphic studies will provide fruitful information on the diversity of marine reptiles and selachians within the Gantour "C2" level.

In addition, the Gantour selachian fauna may provide unknown insights into the evolution of Squaliform lineages across the Mediterranean Tethys. For example, the first appearance of *Squalus aff. huntensis* in the "SX" level has traditionally been interpreted as late Maastrichtian (Bardet et al., 2017). However, our refined stratigraphy implies that species in this genus likely underwent further radiation after the K–Pg transition. In addition, bony fishes, represented by *Enchodus*, have allowed paleogeographic correlations between the upper and lower Maastrichtian phosphate deposits of the Tethyan marginal ocean domain using biostratigraphy (Bardet et al., 2017; Cappetta et al., 2014). Consequently, the presence of *Enchodus* species in the "SX" level (Cappetta et al., 2014), here dated to the Danian instead of the late Maastrichtian, indicates that caution should be taken when using these specimens as correlative biostratigraphic tools. According to our data, *Enchodus* specimens, like many other actinopterygians, successfully crossed the K–Pg boundary in the Gantour basin. Importantly, our new stratigraphy does not generate a paleontological paradox in which extinct Cretaceous species like *mosasaurids* are found in Paleogene sediments. Moreover, our $\delta^{13}C_{org}$ chemostratigraphic results constrain the evolution of shark species preserved in the Gantour "C0" level to the late Danian.

Selachian taxa are known to document their evolution at the K–Pg transition (e.g., Noubhani and Cappetta, 1997). Many of the selachian lineages that began to diversify during the Paleogene have contributed towards clarifying the global evolutionary patterns of vertebrates (Lebrun, 2020). In particular, Paleogene rocks of the NW Moroccan phosphate basins are defined on the basis of their diverse selachian faunas (Bardet et al., 2017; Noubhani and Cappetta, 1997). Thus, recognition of the Selandian Stage in the Gantour basin provides helpful correlative and biostratigraphic tools for comparative studies of western central African fossiliferous localities where selachians, among other vertebrates, have been reported (Solé et al., 2019). In this regard, our $\delta^{13}C_{org}$ chemostratigraphic results for the western Gantour phosphate sequence should promote important discussions on the paleoecological and paleobiogeographic implications of vertebrate faunal biodiversity and evolution during the Paleocene. This, in turn, will greatly expand our ability to reconstruct and appreciate the factors that enabled the distribution and exchange of faunal assemblages between the Tethyan Sea and central Africa.

Conclusions and perspectives

$\delta^{13}C_{org}$ chemostratigraphy provides convincing evidence for phosphate deposition in the upper phosphate series of the western Gantour basin over ~8.5 Myr. Particularly, our results confirm the potential of $\delta^{13}C_{org}$ chemostratigraphy as a powerful tool for refining the stratigraphy of the NW Moroccan phosphate basins. Long-term negative and positive $\delta^{13}C_{org}$ trends are recorded from the K–Pg transition to the mid-Thanetian. Based on our comparison of the absolute $\delta^{13}C$ variations between the global $\delta^{13}C_{carb}$ and Gantour $\delta^{13}C_{org}$ values, the phosphate-bearing rocks may preserve transient CIEs related to the meteorite impact at the K–Pg transition or the LDE, though this latter proposition requires further investigation at higher sampling resolution. Nonetheless, for the first time, our results reliably locate the base of the Danian Stage and constrain the potential presence of Selandian Stage rocks and the PCIM in the western Gantour basin. Importantly, these conclusions are consistent with previous worldwide biostratigraphic determinations of some Maastrichtian vertebrate groups that were wiped out during the K–Pg extinction event. For instance, the Paleocene evolution of primitive placental mammals can be reasonably associated with the Gantour basin on the basis of our proposed $\delta^{13}C_{org}$ model. If this stratigraphic placement is correct, then the Gantour vertebrate taxa may reveal new marine connections between north Africa, the Tethyan paleogeographic domain, and central Africa during the Paleocene, enhancing our knowledge of the paleobiogeographic distribution of biodiversity and their connectivity during this important geological window. For example, the well-calibrated NW Moroccan phosphate sections from the western Gantour and Ouled Abdoun basins may prove useful to better constraining their basinal stratigraphic correlation and interpretation. Furthermore, such results will aid attempts to decipher the allocyclic processes and controls that might have been crucial in shaping phosphate sedimentation in NW Morocco. Finally, the well-documented sequence stratigraphic framework in the MHA may now allow the identification of a major maximum flooding zone across this basin, previously dated to the Selandian-Thanetian transition (El Bamiki et al., 2020).

Acknowledgments

We deeply acknowledge the support of Mohammed VI Polytechnic University (UM6P), University of Montpellier (UM) [UM6P-UM specific agreement n° UM 190775 relating to the UM6P-UM/CNRS framework agreement n° UM 190759], and Office Chérifien des Phosphates (OCP) S.A. [OCP-UM6P specific agreement n° 7 "Multi-scale distribution of minor and trace elements in Moroccan phosphate deposits" relating to the OCP-UM6P framework agreement in Sciences & Technology]. All parties are warmly thanked for the whole scientific cooperation agreement. We are grateful to Jamal Amalik, OCP Innovation, as he provided constant help and support for collaborative projects between OCP, UM6P, and UM. For scientific discussions, Sylvain Adnet (University of Montpellier) and Johan Yans (University of Namur) are thanked. We thank Robert Dennen (RD Editing Services) for improving the English of the paper.

References

Arambourg, C., 1935. Note préliminaire sur les vertébrés fossiles des phosphates du Maroc. Bulletin de la Société Géologique de France 5, 413–439.

Arambourg, C., 1952. Les vertébrés fossiles des gisements de phosphates (Maroc-Algérie-Tunisie). Notes et Memoires du Service Geologique du Maroc 92, 1–372.

Aubineau, J., Parat, F., Chi Fru, E., El Bamiki, R., Mauguin, O., Baron, F., Poujol, M., Séranne, M., 2022a. Geodynamic seawater-sediment porewater evolution of the east central Atlantic Paleogene ocean margin revealed by U-Pb dating of sedimentary phosphates. Frontiers in Earth Science 10.

Aubineau, J., Parat, F., Elghali, A., Raji, O., Addou, A., Bonnet, C., Muñoz, M., Mauguin, O., Baron, F., Jouti, M.B., Yazami, O.K., Bodinier, J.-L., 2022b. Highly variable content of fluorapatite-hosted CO_3^{2-} in the Upper Cretaceous/Paleogene phosphorites (Morocco) and implications for paleodepositional conditions. Chemical Geology 597, 120818. https://doi.org/10.1016/j.chemgeo.2022.120818

Aubry, M.-P., Ouda, K., Dupuis, C., A, W., Berggren, Couvering, J.A.V., the Members of the Working Group on the Paleocene/Eocene, 2007. The Global Standard Stratotype-section and Point (GSSP) for the base of the Eocene Series in the Dababiya section (Egypt). Episodes Journal of International Geoscience 30, 271–286. https://doi.org/10.18814/epiiugs/2007/v30i4/003

Bardet, N., 2012. Maastrichtian marine reptiles of the Mediterranean Tethys: a palaeobiogeographical approach. Bulletin de la Société Géologique de France 183, 573–596. https://doi.org/10.2113/gssgfbull.183.6.573

Bardet, N., Gheerbrant, E., Noubhani, A., Cappetta, H., Jouve, S., Bourdon, E., Suberbiola, X.P., Jalil, N.-E., Vincent, P., Houssaye, A., Sole, F., Elhoussaini Darif, K., Adnet, S., Rage, J.-C., De Lapparent de Broin, F., Sudre, J., Bouya, B., Amaghzaz, M., Meslouh, S., 2017. Les Vertébrés des phosphates crétacés-paléogènes (72, 1–47, 8 Ma) du Maroc. Mémoire de la Société géologique de France 180, 351–452.

Barnet, J.S.K., Littler, K., Kroon, D., Leng, M.J., Westerhold, T., Röhl, U., Zachos, J.C., 2018. A new high-resolution chronology for the late Maastrichtian warming event: Establishing robust temporal links with the onset of Deccan volcanism. Geology 46, 147–150. https://doi.org/10.1130/G39771.1

Bartley, J.K., Kah, L.C., 2004. Marine carbon reservoir, Corg-Ccarb coupling, and the evolution of the Proterozoic carbon cycle. Geology 32, 129–132. https://doi.org/10.1130/G19939.1

Bodin, S., Charpentier, M., Ullmann, C.V., Rudra, A., Sanei, H., 2023. Carbon cycle during the late Aptian–early Albian OAE 1b: A focus on the Kilian–Paquier levels interval. Global and Planetary Change 222, 104074. https://doi.org/10.1016/j.gloplacha.2023.104074

Bomou, B., Suan, G., Schlögl, J., Grosjean, A.-S., Suchéras-Marx, B., Adatte, T., Spangenberg, J.E., Fouché, S., Zacaï, A., Gibert, C., Brazier, J.-M., Perrier, V., Vincent, P., Janneau, K., Martin, J.E., 2021. The palaeoenvironmental context of Toarcian vertebrate-yielding shales of southern France (Hérault). Geological Society, London, Special Publications 514, 121–152. https://doi.org/10.1144/SP514-2021-16

Boujo, A., 1976. Contribution à l'étude géologique du gisement de phosphate crétacé-éocène des Ganntour (Maroc occidental). Sciences Géologiques, bulletins et mémoires 43.

Cappetta, H., 1987. Extinctions et renouvellements fauniques chez les Sélaciens post-Jurassiques. Mémoires de la Société géologique de France 150, 113–131.

Cappetta, H., Bardet, N., Pereda Suberbiola, X., Adnet, S., Akkrim, D., Amalik, M., Benabdallah, A., 2014. Marine vertebrate faunas from the Maastrichtian phosphates of Benguérir (Ganntour Basin, Morocco): Biostratigraphy, palaeobiogeography and palaeoecology. Palaeogeography, Palaeoclimatology, Palaeoecology 409, 217–238. https://doi.org/10.1016/j.palaeo.2014.04.020

Carignan, J., Hild, P., Mevelle, G., Morel, J., Yeghicheyan, D., 2001. Routine analyses of trace elements in geological samples using flow injection and low pressure on-line liquid chromatography coupled to ICP-MS: a study of geochemical reference materials BR, DR-N, UB-N, AN-G and GH. Geostandards Newsletter 25, 187–198. https://doi.org/10.1111/j.1751-908X.2001.tb00595.x

Charton, R., Bertotti, G., Arnould, A.D., Storms, J.E.A., Redfern, J., 2021. Low- temperature thermochronology as a control on vertical movements for semi- quantitative source- to- sink analysis: A case study for the Permian to Neogene of Morocco and surroundings. Basin Research 33, 1337–1383. https://doi.org/10.1111/bre.12517

Coccioni, R., Frontalini, F., Bancalà, G., Fornaciari, E., Jovane, L., Sprovieri, M., 2010. The Dan-C2 hyperthermal event at Gubbio (Italy): Global implications, environmental effects, and cause(s). Earth and Planetary Science Letters 297, 298–305. https://doi.org/10.1016/j.epsl.2010.06.031

Cramer, B.D., Saltzman, M.R., 2007. Early Silurian paired $\delta^{13}C_{carb}$ and $\delta^{13}C_{org}$ analyses from the Midcontinent of North America: Implications for paleoceanography and paleoclimate. Palaeogeography, Palaeoclimatology, Palaeoecology, Neoproterozoic to Paleozoic Ocean Chemistry 256, 195–203. https://doi.org/10.1016/j.palaeo.2007.02.032

Dewalque, C., 1868. Prodrome d'une description geologique de la Belgique. Librairie Polytechnique De Decq, Bruxelles and Liege.

Dickens, G.R., Castillo, M.M., Walker, J.C.G., 1997. A blast of gas in the latest Paleocene: Simulating first-order effects of massive dissociation of oceanic methane hydrate. Geology 25, 259–262. https://doi.org/10.1130/0091-7613(1997)025<0259:ABOGIT>2.3.CO;2

Döebelin, N., Kleeberg, R., 2015. Profex: a graphical user interface for the Rietveld refinement program BGMN. J Appl Cryst 48, 1573–1580. https://doi.org/10.1107/S1600576715014685

Domingo, L., López-Martínez, N., Leng, M.J., Grimes, S.T., 2009. The Paleocene–Eocene Thermal Maximum record in the organic matter of the Claret and Tendruy continental sections (South-central Pyrenees, Lleida, Spain). Earth and Planetary Science Letters 281, 226–237. https://doi.org/10.1016/j.epsl.2009.02.025

El Bamiki, R., Raji, O., Ouabid, M., Elghali, A., Khadiri Yazami, O., Bodinier, J.-L., 2021. Phosphate Rocks: A Review of Sedimentary and Igneous Occurrences in Morocco. Minerals 11, 1137. https://doi.org/10.3390/min11101137

El Bamiki, R., Séranne, M., Chellaï, E.H., Merzeraud, G., Marzoqi, M., Melinte-Dobrinescu, M.C., 2020. The Moroccan High Atlas phosphate-rich sediments: Unraveling the accumulation and differentiation processes. Sedimentary Geology 403, 105655. https://doi.org/10.1016/j.sedgeo.2020.105655

Filippelli, G.M., 1997. Controls on phosphorus concentration and accumulation in oceanic sediments. Marine Geology 139, 231–240. https://doi.org/10.1016/S0025-3227(96)00113-2

Gheerbrant, E., 2009. Paleocene emergence of elephant relatives and the rapid radiation of African ungulates. Proceedings of the National Academy of Sciences 106, 10717–10721. https://doi.org/10.1073/pnas.0900251106

Gheerbrant, E., Sudre, J., Cappetta, H., Bignot, G., 1998. *Phosphatherium escuilliei* du Thanétien du Basin des Ouled Abdoun (Maroc), plus ancien proboscidien (Mammalia) d'Afrique. Geobios 30, 247–269.

Gheerbrant, E., Sudre, J., Cappetta, H., Mourer-Chauviré, C., Bourdon, E., Iarochene, M., Amaghzaz, M., Bouya, B., 2003. The mammal localities of Grand Daoui Quarries, Ouled Abdoun Basin, Morocco, Ypresian : A first survey. Bull. Soc. géol. Fr 174, 279–293. https://doi.org/10.2113/174.3.279

Glenn, C.R., Föllmi, K., Riggs, S.R., Baturin, G.N., Grimm, K.A., Trappe, J., Abed, A.M., Galli-Olivier, C., Garrison, R.E., Ilyin, A.V., Jehn, C., Rohrlich, V., Sadakah, R.M.Y., Schidlowski, M., Sheldon, R.E., Siegmund, H., 1994. Phosphorus and phosphorites: Sedimentology and environments of formation. Eclogae geol. Helv 87, 747–788. https://doi.org/0012-9402194/030747-42

J.M. Hayes, I.R. Kaplan, K.W. Wedeking, Precambrian organic geochemistry, preservation of the record, in: J.W. Schopf (Ed.), The Earth's Earliest Biosphere: Its Origin and Evolution, Princeton University Press, Princeton, N.J., 1983, pp. 93–134.

Hollard, H., Choubert, G., Bronner, G., Marchand, J., Sougy, J., 1985. Carte géologique du Maroc. Échelle 1/1 000 000.

Jeanmaire, J.-P., 1985. Répartition de l'uranium dans les niveaux phosphatés Maestrichtien Supérieur - Eocène Inférieur du secteur de Benguerir (Bassin des Ganntour, Maroc occidental). Sciences Géologiques, bulletins et mémoires 77, 53–68.

Jiang, G., Wang, X., Shi, X., Xiao, S., Zhang, S., Dong, J., 2012. The origin of decoupled carbonate and organic carbon isotope signatures in the early Cambrian (ca. 542–520Ma) Yangtze platform. Earth and Planetary Science Letters 317–318, 96–110. https://doi.org/10.1016/j.epsl.2011.11.018

Kennett, J.P., Stott, L.D., 1991. Abrupt deep-sea warming, palaeoceanographic changes and benthic extinctions at the end of the Palaeocene. Nature 353, 225–229.

Knoll, A.H., Hayes, J.M., Kaufman, A.J., Swett, K., Lambert, I.B., 1986. Secular variation in carbon isotope ratios from Upper Proterozoic successions of Svalbard and East Greenland. Nature 321, 832–838. https://doi.org/10.1038/321832a0

Koch, P.L., Zachos, J.C., Gingerich, P.D., 1992. Correlation between isotope records in marine and continental carbon reservoirs near the Palaeocene/Eocene boundary. Nature 358, 319–322. https://doi.org/10.1038/358319a0

Kocsis, L., Gheerbrant, E., Mouflih, M., Cappetta, H., Yans, J., Amaghzaz, M., 2014. Comprehensive stable isotope investigation of marine biogenic apatite from the late Cretaceous–early Eocene phosphate series of Morocco. Palaeogeography, Palaeoclimatology, Palaeoecology 394, 74–88. https://doi.org/10.1016/j.palaeo.2013.11.002

Korte, C., Kozur, H.W., 2010. Carbon-isotope stratigraphy across the Permian–Triassic boundary: A review. Journal of Asian Earth Sciences 39, 215–235. https://doi.org/10.1016/j.jseaes.2010.01.005

Lebrun, P., 2020. Fossils from Morocco. Volume IIa. Emblematic localities from the Mesozoic and the Palaeogene, Les Editions du Piat. ed. Saint-Julien-du-Pinet.

Li, L., Keller, G., 1998a. Abrupt deep-sea warming at the end of the Cretaceous. Geology 26, 995–998. https://doi.org/10.1130/0091-7613(1998)026<0995:ADSWAT>2.3.CO;2

Li, L., Keller, G., 1998b. Maastrichtian climate, productivity and faunal turnovers in planktic foraminifera in South Atlantic DSDP sites 525A and 21. Marine Micropaleontology 33, 55–86. https://doi.org/10.1016/S0377-8398(97)00027-3

Littler, K., Röhl, U., Westerhold, T., Zachos, J.C., 2014. A high-resolution benthic stable-isotope record for the South Atlantic: Implications for orbital-scale changes in Late Paleocene–Early Eocene climate and carbon cycling. Earth and Planetary Science Letters 401, 18–30. https://doi.org/10.1016/j.epsl.2014.05.054

Lucas, J., Prévôt-Lucas, L., 1995. Tethyan Phosphates and Bioproductites, in: Nairn, A.E.M., Ricou, L.-E., Vrielynck, B., Dercourt, J. (Eds.), The Tethys Ocean. Springer, Boston, MA, pp. 367–391. https://doi.org/10.1007/978-1-4899-1558-0_12

McClellan, G.H., 1980. Mineralogy of carbonate fluorapatites. Journal of the Geological Society 137, 675–681.

McClellan, G.H., Van Kauwenbergh, S.J., 1991. Mineralogical and chemical variation of francolites with geological time. Journal of the Geological Society 148, 809–812.

https://doi.org/10.1144/gsjgs.148.5.0809

Meunier, A., 2005. Clays. Springer, Berlin ; New York.

Meyer, K.M., Yu, M., Lehrmann, D., van de Schootbrugge, B., Payne, J.L., 2013. Constraints on Early Triassic carbon cycle dynamics from paired organic and inorganic carbon isotope records. Earth and Planetary Science Letters 361, 429–435. https://doi.org/10.1016/j.epsl.2012.10.035

Michard, A., Saddiqi, O., Chalouan, A., Frizon de Lamotte, D., 2008. Continental Evolution: The Geology of Morocco. Springer, Berlin, Heidelberg.

Mouflih, M., 2015. Les phosphates du Maroc central et du Moyen Atlas (Maastrichtien-Lutetien, Maroc): Sedimentologie, stratigraphie sequentielle, contexte genetique et valorisation. Université de Cadi Ayyad, Marrakech.

Nathan, Y., 1984. The Mineralogy and Geochemistry of Phosphorites, in: Nriagu, J.O., Moore, P.B. (Eds.), Phosphate Minerals. Springer-Verlag, Berlin, Heidelberg, pp. 275–291.

Noiret, C., Steurbaut, E., Tabuce, R., Marandat, B., Schnyder, J., Storme, J.-Y., Yans, J., 2016. New bio-chemostratigraphic dating of a unique early Eocene sequence from southern Europe results in precise mammalian biochronological tie-points. Newsletters on Stratigraphy 49, 469–480. https://doi.org/10.1127/nos/2016/0336

Noubhani, A., 2010. The selachians' faunas of the Moroccan phosphate deposits and the KT mass-extinctions. Historical Biology 22, 71–77. https://doi.org/10.1080/08912961003707349

Noubhani, A., Cappetta, H., 1997. Les Orectolobiformes, Carcharhiniformes et Myliobatiformes (Elasmobranchii, Neoselachii) des Bassins a phosphate du Maroc (Maastrichtien-Lutetien basal) : systematique, biostratigraphie, evolution et dynamique des faunes. Palaeo Ichthyologica 8.

OCP, 1989. The phosphate basins of Morocco, in: Notholt, A.J.G., Sheldon, R.P., Davidson, D.F. (Eds.), Phosphate Deposits of the World, Vol. 2: Phosphate Rock Resources. Cambridge, United Kingdom, pp. 301–311.

Oehlert, A.M., Swart, P.K., 2014. Interpreting carbonate and organic carbon isotope covariance in the sedimentary record. Nat Commun 5, 4672. https://doi.org/10.1038/ncomms5672

Ollivier-Pierre, M.-F., 1982. La microflore du Paléocène et de l'Eocène des séries phosphatées des Ganntour (Maroc). Sci. Géol. Bull 35, 117–127. https://doi.org/10.3406/sgeol.1982.1615

Pan, Y., Fleet, M.E., 2002. Compositions of the Apatite-Group Minerals: Substitution Mechanisms and Controlling Factors. Reviews in Mineralogy and Geochemistry 48, 13–49. https://doi.org/10.2138/rmg.2002.48.2

Pufahl, P.K., Groat, L.A., 2017. Sedimentary and Igneous Phosphate Deposits: Formation and Exploration: An Invited Paper. Economic Geology 112, 483–516. https://doi.org/10.2113/econgeo.112.3.483

Rauscher, R., Doubinger, J., 1982. Les dinokystes du Maestrichtien phosphaté du Maroc. Sci. Géol. Bull 35, 97–116. https://doi.org/10.3406/sgeol.1982.1614

Rothman, D.H., Hayes, J.M., Summons, R.E., 2003. Dynamics of the Neoproterozoic carbon cycle. Proceedings of the National Academy of Sciences 100, 8124–8129.

Ruttenberg, K.C., 2003. The Global Phosphorus Cycle, in: Schlesinger, W.H. (Ed.), Treatise on Geochemistry, Vol. 8. Elsevier Ltd, pp. 585–643.

Salvan, H., 1955. Les invertébrés fossiles des phosphates marocains. Notes et Memoires du Service Geologique du Maroc 93, 1–258.

Schmitz, B., Pujalte, V., Molina, E., Monechi, S., Orue-Etxebarria, X., Speijer, R.P., Alegret, L., Apellaniz, E., Arenillas, I., Aubry, M.-P., Baceta, J.-I., Berggren, W.A., Bernaola, G., Caballero, F., Clemmensen, A., Dinarès-Turell, J., Dupuis, C., Heilmann-Clausen, C., Orús, A.H., Knox, R., Martín-Rubio, M., Ortiz, S., Payros, A., Petrizzo, M.R., von Salis, K., Sprong, J., Steurbaut, E., Thomsen, E., 2011. The Global Stratotype Sections and Points for the bases of the Selandian (Middle Paleocene) and Thanetian (Upper Paleocene) stages at Zumaia, Spain. Episodes Journal of International Geoscience 34, 220–243. https://doi.org/10.18814/epiiugs/2011/v34i4/002

Sluijs, A., Dickens, G.R., 2012. Assessing offsets between the δ13C of sedimentary components and the global exogenic carbon pool across early Paleogene carbon cycle perturbations. Global Biogeochemical Cycles 26. https://doi.org/10.1029/2011GB004224

Solé, F., Noiret, C., Desmares, D., Adnet, S., Taverne, L., De Putter, T., Mees, F., Yans, J., Steeman, T., Louwye, S., Folie, A., Stevens, N.J., Gunnell, G.F., Baudet, D., Yaya, N.K., Smith, T., 2019. Reassessment of historical sections from the Paleogene marine margin of the Congo Basin reveals an almost complete absence of Danian deposits. Geoscience Frontiers, Special Issue: Advances in Himalayan Tectonics 10, 1039–1063. https://doi.org/10.1016/j.gsf.2018.06.002

Środoń, J., Eberl, D.D., 1984. Illite, in: Bailey, S.W. (Ed.), Review in Mineralogy Vol. 13, Micas. Mineralogical Society of America, Washington DC, pp. 495–544.

Stap, L., Lourens, L.J., Thomas, E., Sluijs, A., Bohaty, S., Zachos, J.C., 2010. High-resolution deep-sea carbon and oxygen isotope records of Eocene Thermal Maximum 2 and H2. Geology 38, 607–610. https://doi.org/10.1130/G30777.1

Storme, J.-Y., Devleeschouwer, X., Schnyder, J., Cambier, G., Baceta, J.I., Pujalte, V., Di Matteo, A., Iacumin, P., Yans, J., 2012. The Palaeocene/Eocene boundary section at Zumaia (Basque-Cantabric Basin) revisited: new insights from high-resolution magnetic susceptibility and carbon isotope chemostratigraphy on organic matter ($\delta^{13}C_{org}$). Terra Nova 24, 310–317. https://doi.org/10.1111/j.1365-3121.2012.01064.x

Svensen, H., Planke, S., Malthe-Sørenssen, A., Jamtveit, B., Myklebust, R., Rasmussen Eidem, T., Rey, S.S., 2004. Release of methane from a volcanic basin as a mechanism for initial Eocene global warming. Nature 429, 542–545. https://doi.org/10.1038/nature02566

Thibault, N., Harlou, R., Schovsbo, N.H., Stemmerik, L., Surlyk, F., 2016. Late Cretaceous (late Campanian–Maastrichtian) sea-surface temperature record of the Boreal Chalk Sea. Climate of the Past 12, 429–438. https://doi.org/10.5194/cp-12-429-2016

Thomas, E., Zachos, J.C., 2000. Was the late Paleocene thermal maximum a unique event? GFF 122, 169–170. https://doi.org/10.1080/11035890001221169

Tribovillard, N., Algeo, T.J., Lyons, T., Riboulleau, A., 2006. Trace metals as paleoredox and paleoproductivity proxies: An update. Chemical Geology 232, 12–32. https://doi.org/10.1016/j.chemgeo.2006.02.012

Van der Beek, P., Mbede, E., Andriessen, P., Delvaux, D., 1998. Denudation history of the Malawi and Rukwa Rift flanks (East African Rift System) from apatite fission track thermochronology. Journal of African Earth Sciences, Tectonics, Sedimentation and Volcanism in the East African Rift System 26, 363–385. https://doi.org/10.1016/S0899-5362(98)00021-9

Vandenberghe, N., Hilgen, F.J., Speijer, R., 2012. The Paleogene Period, in: Gradstein, F.M., Ogg, J.G., Schmitz, M.D., Ogg, G.M. (Eds.), The Geological Time Scale 2012. Elsevier, Oxford, pp. 855–921.

Velde, B., Suzuki, T., Nicot, E., 1986. Pressure-temperature-composition of illite/smectite mixed-layer minerals: Niger delta mudstones and other examples. Clays and Clay Minerals 34, 435–441.

Westerhold, T., Marwan, N., Drury, A.J., Liebrand, D., Agnini, C., Anagnostou, E., Barnet, J.S.K., Bohaty, S.M., De Vleeschouwer, D., Florindo, F., Frederichs, T., Hodell, D.A., Holbourn, A.E., Kroon, D., Lauretano, V., Littler, K., Lourens, L.J., Lyle, M., Pälike, H., Röhl, U., Tian, J., Wilkens, R.H., Wilson, P.A., Zachos, J.C., 2020. An astronomically dated record of Earth’s climate and its predictability over the last 66 million years. Science 369, 1383–1387. https://doi.org/10.1126/science.aba6853

Westerhold, T., Röhl, U., Donner, B., McCarren, H.K., Zachos, J.C., 2011. A complete high-resolution Paleocene benthic stable isotope record for the central Pacific (ODP Site 1209). Paleoceanography 26. https://doi.org/10.1029/2010PA002092

Yans, J., Amaghzaz, M., Bouya, B., Cappetta, H., Iacumin, P., Kocsis, L., Mouflih, M., Selloum, O., Sen, S., Storme, J.-Y., Gheerbrant, E., 2014. First carbon isotope chemostratigraphy of the Ouled Abdoun phosphate Basin, Morocco; implications for dating and evolution of earliest African placental mammals. Gondwana Research 25, 257–269. https://doi.org/10.1016/j.gr.2013.04.004

Young, S.A., Saltzman, M.R., Bergström, S.M., Leslie, S.A., Xu, C., 2008. Paired $\delta^{13}C_{carb}$ and $\delta^{13}C_{org}$ records of Upper Ordovician (Sandbian–Katian) carbonates in North America and China: Implications for paleoceanographic change. Palaeogeography, Palaeoclimatology, Palaeoecology 270, 166–178. https://doi.org/10.1016/j.palaeo.2008.09.006

Zachos, J., Pagani, M., Sloan, L., Thomas, E., Billups, K., 2001. Trends, rhythms, and aberrations in global climate 65 Ma to present. Science 292, 686–693.

Zachos, J.C., Arthur, M.A., Dean, W.E., 1989. Geochemical evidence for suppression of pelagic marine productivity at the Cretaceous/Tertiary boundary. Nature 337, 61–64. https://doi.org/10.1038/337061a0

Zachos, J.C., Dickens, G.R., Zeebe, R.E., 2008. An early Cenozoic perspective on greenhouse warming and carbon-cycle dynamics. Nature 451, 279–283. https://doi.org/10.1038/nature06588

Figure and Table captions

Figure 1. Study locality, lithology, and stratigraphy. (**a**) Spatial distribution of the Upper Cretaceous–Paleogene phosphate basins (orange) in northwestern Morocco. (**b**) Simplified geological map of the Gantour and Ouled Abdoun phosphorus-rich basins (adopted from Hollard et al., 1985). The yellow star indicates the studied 6258 mining well (Bouchane section), and the yellow circles display other studied sections: 1, Bout El Mezoud (Noubhani and Cappetta, 1997); 2, well 88 (Jeanmaire, 1985); 3, El Borouj (Boujo, 1976); 4, Recette IV (Gheerbrant et al., 2003; Noubhani and Cappetta, 1997); 5, P7 (Kocsis et al., 2014); 6, RP 13-2 (Gheerbrant et al., 2003); 7, SDA-06-02 (Yans et al., 2014). These sections are presented in Figure 6.

Figure 2. Lithology and stratigraphy. Synthetic lithostratigraphic column of the 6258 mining well in the western Gantour phosphate series. Interbasinal stratigraphic correlations between the Bouchane P-bearing rocks and those from other published sections (Youssoufia and Benguerir zones; OCP, 1989) were performed by OCP geologists. Consequently, the studied interval presumably covers the upper Maastrichtian–Thanetian (OCP, 1989). The OCP group currently exploits the crumbly phosphorite beds. $†_1$: Numerous Ypresian Orectolobiformes, Carcharhiniformes, and Myliobatiformes (selachians) overlying the "SFA" level are described and correlated with European strata (Noubhani and Cappetta, 1997). $†_2$: *Palaeogaleus brivesi* and other Selachian species (<10) are preserved in the Gantour "C0–C1" level and correlated with European Danian rocks (Noubhani and Cappetta, 1997). $†_3$: Last occurrence of many Cretaceous marine reptiles and selachian families in the Gantour C2 level. Stratigraphic subdivisions and sampling positions within the Gantour "C2" level are not reported (Cappetta et al., 2014). See discussion for further details.

Figure 3. Deciphering the origin of organic matter. (**a**) Mineral composition and relative abundance of the bulk fraction (measured by XRD) through the studied phosphate-bearing section. (**b**) Relationships between TOC/Si and Al_2O_3, TiO_2, and P_2O_5, as well as between Al_2O_3 and P_2O_5.

Figure 4. $\delta^{13}C_{org}$ and TOC curves of the studied section (6258 well, western Gantour basin). The unrefined stratigraphy is based on OCP (1989) data, whereas the refined

stratigraphy (this work) is based on correlations with calibrated reference sections (see Fig. 5). The presented mining levels exclusively correlate within the Gantour basin. Red arrows indicate the position of each sample. The inset plot shows the weak correlation between $\delta^{13}C_{org}$ and TOC. Maast, Maastrichtian; VPDB, Vienna Peedee belemnite.

Figure 5. Correlation scheme of the Paleocene interval in the western Gantour area using $\delta^{13}C$ chemostratigraphy. The Bouchane section (this work) is correlated to reference sections calibrated to the geomagnetic polarity and biostratigraphic scales (Li and Keller, 1998a, 1998b; Westerhold et al., 2020; Yans et al., 2014). The “C0–C1” level hosts Danian sharks (see Section 2.2), which enabled the initial stratigraphic placement of our $\delta^{13}C_{org}$ curve with respect to the global $\delta^{13}C_{carb}$ curve. This approach aims to supersede the poorly resolved stratigraphy published by OCP (1989) and shown in Figure 4. Light gray shading indicates the upward negative trend from the K–Pg transition to the minimum isotopic value, whereas dark shading indicates the upward positive trend until the PCIM. Geomagnetic polarity state is indicated as normal in black and reverse in white. Paleogene Zonations (NP Zones) are replotted from Vandenberghe et al. (2012). Lut, Lutetian; LME, Late Maastrichtian Event; MI K–Pg, Meteorite Impact Cretaceous-Paleogene; LDE, Latest Danian Event; PCIM, Paleocene Carbon Isotope Maximum; PETM, Paleocene-Eocene Thermal Maximum; EECO, Early Eocene Climate Optimum; ETM, Eocene Thermal Maximum; VPDB, Vienna Peedee belemnite. The Cenozoic global reference benthic foraminifer carbon isotope dataset, the most recent astronomically tuned, high-definition stratigraphic reference, is redrafted from Westerhold et al. (2020), whereas the $\delta^{13}C_{carb}$ trend from 72.1 to 67 Ma is modified from Thibault et al. (2016). Westerhold et al. (2020) reported both short-term (black) and long-term (red) trends that were smoothed over 20 kyr and 1 Myr increments, respectively using a locally weighted function.

Figure 6. Stratigraphic correlations of the NW Moroccan phosphate sequence between the Gantour, Ouled Abdoun, and Marrakesh High Atlas basins based on $\delta^{13}C_{org}$ data from the Bouchane and Sidi Daoui sections and existing biostratigraphic data from calcareous nannofossils. Phosphate-bearing sequences are grouped based on whether (**a**) age constraints are available or (**b**) no age constraints are available. The PCIM, preserved within the western Gantour “SFA1S” and Ouled Abdoun “C2a”

levels, is the reference datum for horizontalization. The K–Pg transition is preserved within the Gantour "C2M" level, but stratigraphic subdivisions of the "C2" level are lacking in the eastern Gantour basin. Mining names of phosphorite horizons following the nomenclature of the mine workers are not equivalent between basins, but are likely identical within the same basin. Synthetic lithostratigraphic columns are modified from El Bamiki et al. (2021, 2020); Gheerbrant et al. (2003); Jeanmaire (1985); Kocsis et al. (2014); and Yans et al. (2014). The yellowish marls are a marker level within the Gantour basin (Noubhani and Cappetta, 1997; OCP, 1989). Note different vertical scales for the Amizmiz, RP13-2, and P7 sections. U.T., Upper Thanetian; Maast, Maastrichtian.

Table 1. Organic carbon isotope compositions ($\delta^{13}C_{org}$) and total organic carbon (TOC) contents for all samples in this study. VPDB, Vienna Peedee belemnite.

Figure 1

Click here to access/download;Figure;Figure 1 -

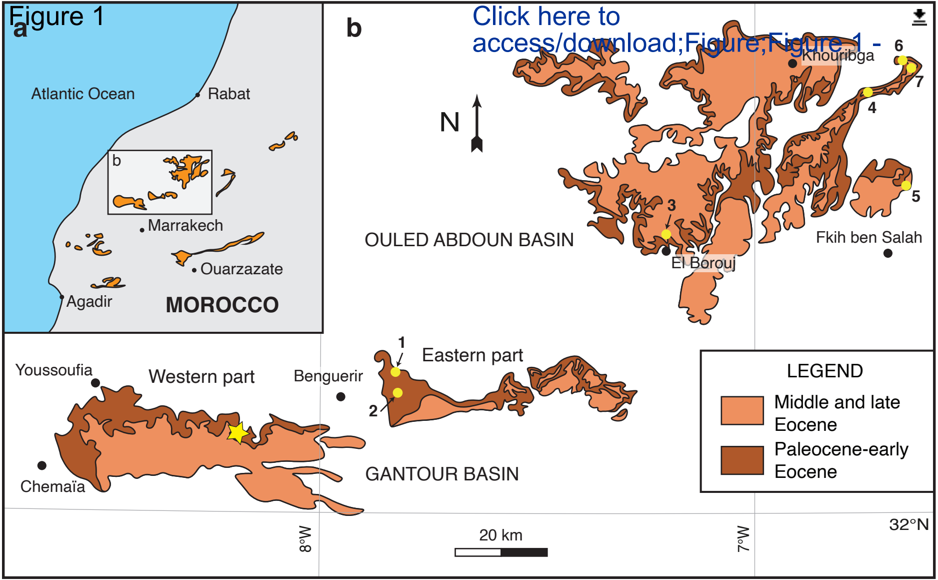

Figure 2

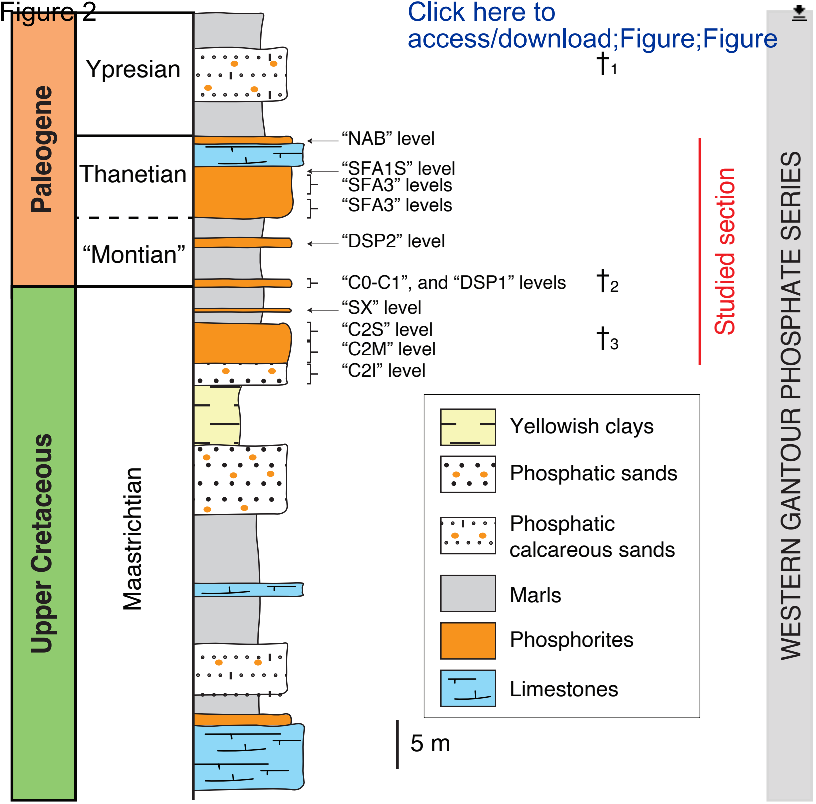

Paleogene
Upper Cretaceous
Ypresian
Thanetian
"Montian"
Maastrichtian
"NAB" level
"SFA1S" level
"SFA3" levels
"SFA3" levels
"DSP2" level
"C0-C1", and "DSP1" levels
"SX" level
"C2S" level
"C2M" level
"C2I" level
†1
†2
†3
Studied section
WESTERN GANTOUR PHOSPHATE SERIES
Yellowish clays
Phosphatic sands
Phosphatic calcareous sands
Marls
Phosphorites
Limestones
5 m

Figure 3

Click here to access/download;Figure;Figure 3.pdf

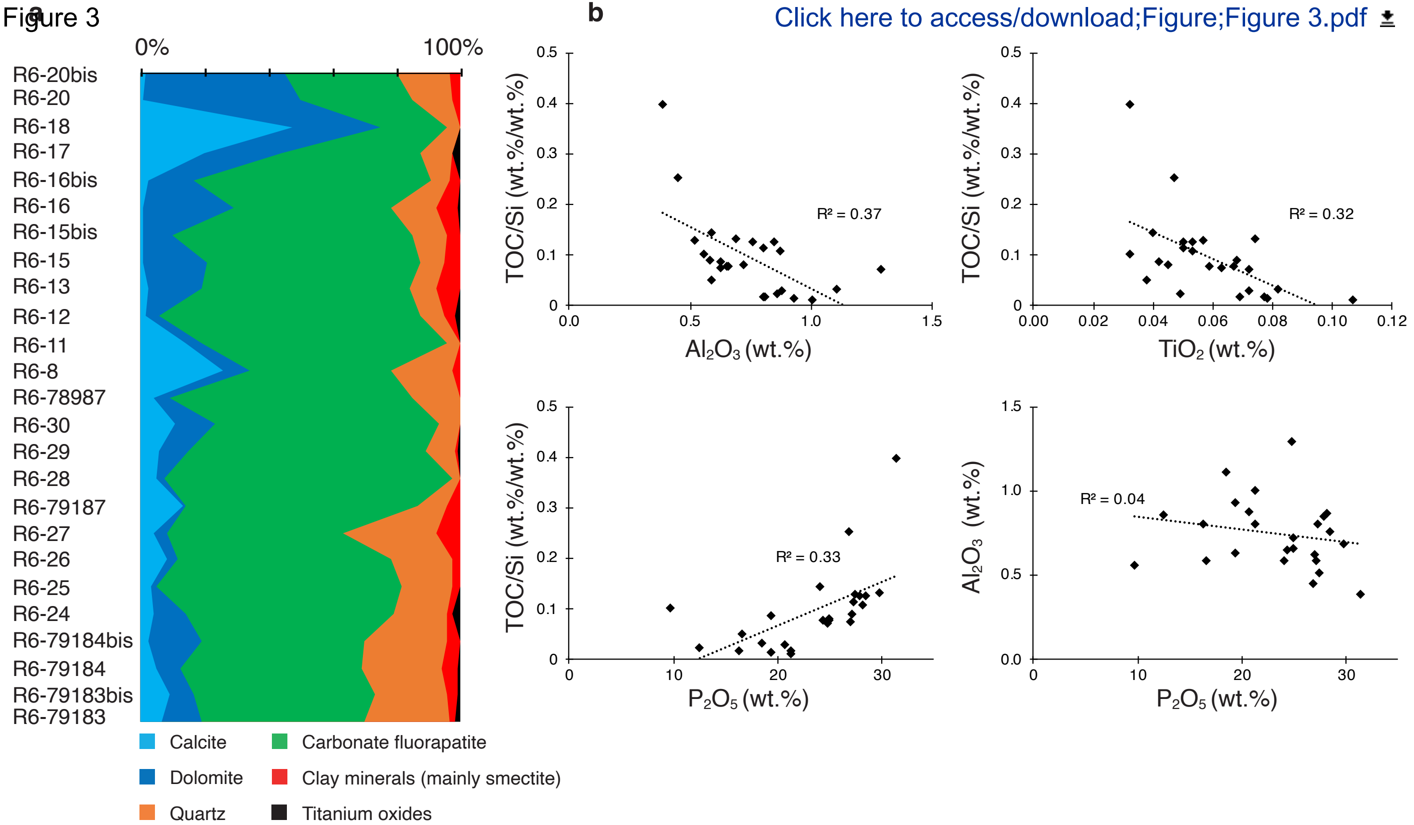

Figure 4

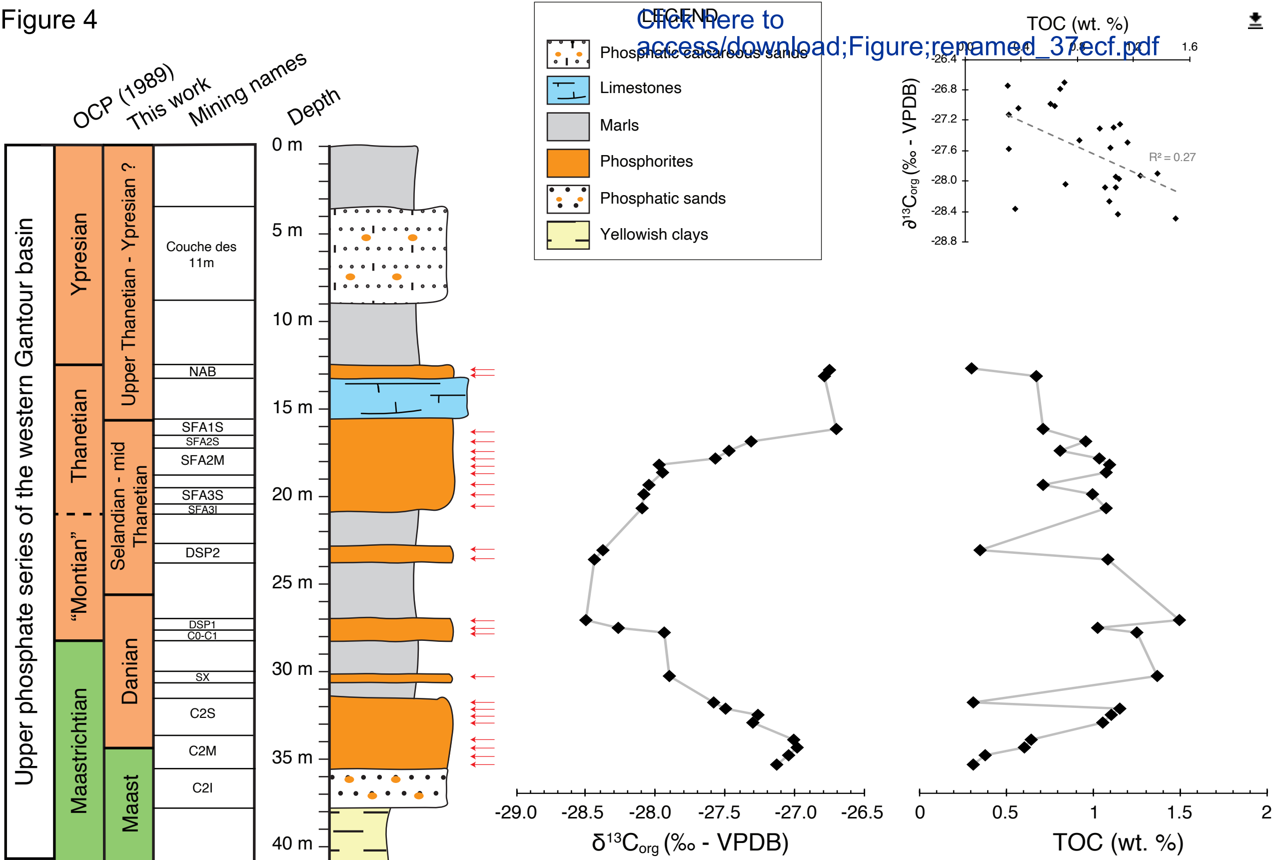
OCP (1989)
This work
Mining names
Depth
Upper phosphate series of the western Gantour basin
Ypresian
Thanetian
"Montian"
Maastrichtian
Upper Thanetian - Ypresian ?
Selandian - mid Thanetian
Danian
Maast
Couche des 11m
NAB
SFA1S
SFA2S
SFA2M
SFA3S
SFA3I
DSP2
DSP1
C0-C1
SX
C2S
C2M
C2I
0 m
5 m
10 m
15 m
20 m
25 m
30 m
35 m
40 m
LEGEND
Phosphatic calcareous sands
Limestones
Marls
Phosphorites
Phosphatic sands
Yellowish clays
TOC (wt. %)
0.0
0.4
0.8
1.2
1.6
-26.4
-26.8
-27.2
-27.6
-28.0
-28.4
-28.8
δ13Corg (‰ - VPDB)
R² = 0.27
-29.0
-28.5
-28.0
-27.5
-27.0
-26.5
δ13Corg (‰ - VPDB)
0
0.5
1
1.5
2
TOC (wt. %)

Figure 5

Click here to access/download;Figure;Figure 5 - Calage temporelle.pdf

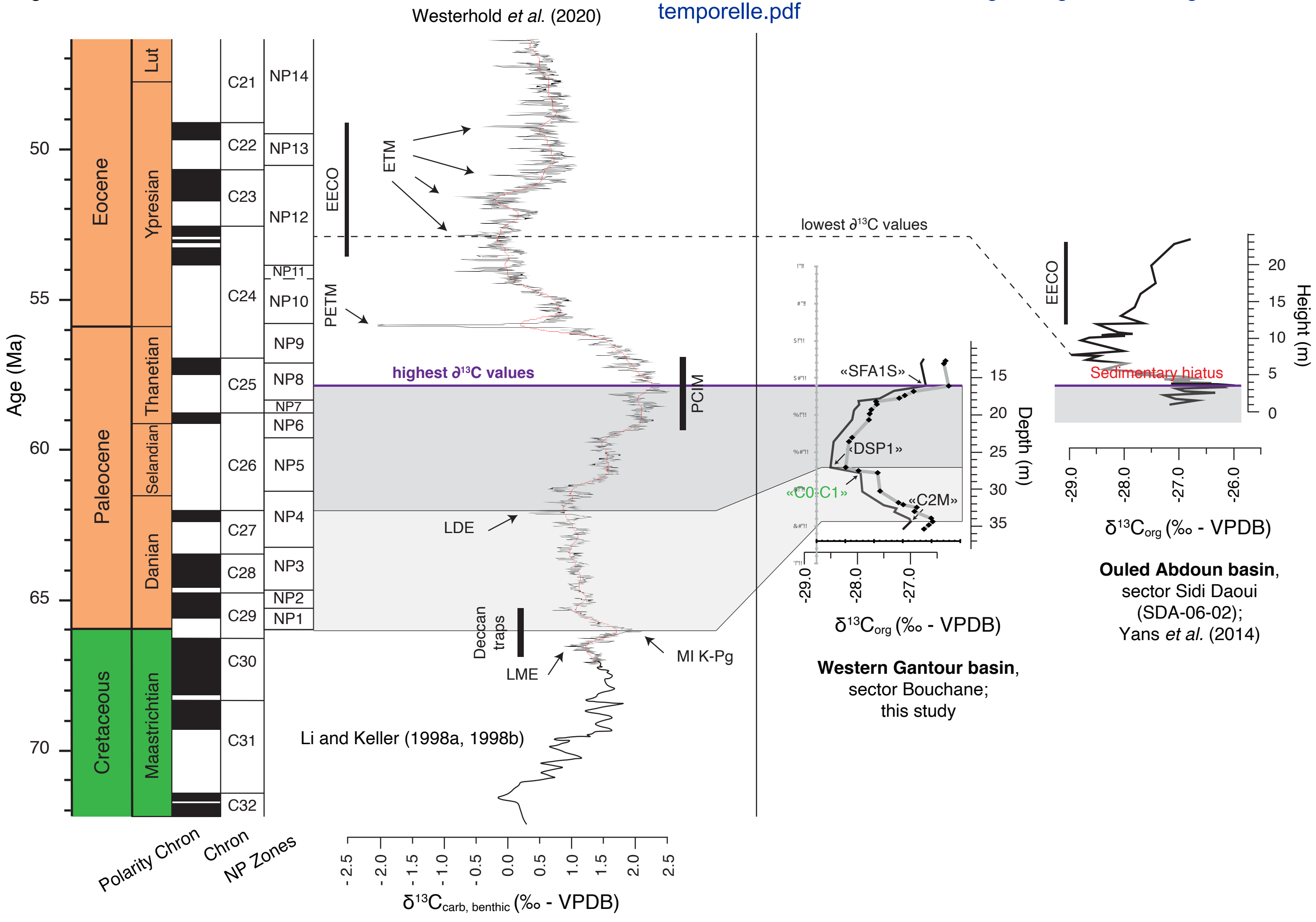

Figure 6

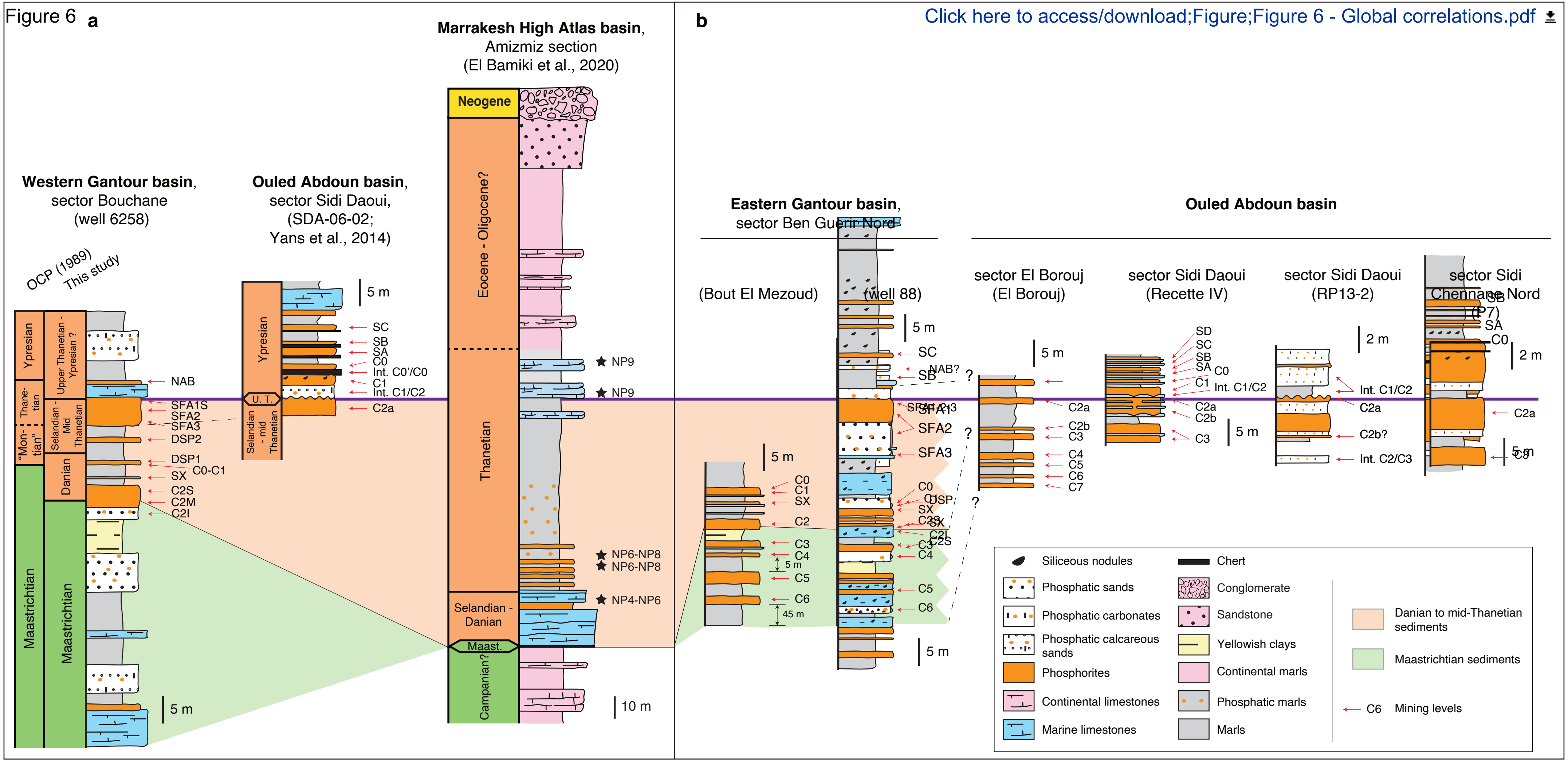

a
Western Gantour basin, sector Bouchane (well 6258)
OCP (1989)
This study
Ouled Abdoun basin, sector Sidi Daoui, (SDA-06-02; Yans et al., 2014)
Marrakesh High Atlas basin, Amizmiz section (El Bamiki et al., 2020)
Neogene
Eocene - Oligocene?
Thanetian
Selandian - Danian
Maast.
Campanian?
Ypresian
Thane-tian
"Mon-tian"
Danian
Maastrichtian
Upper Thanetian - Ypresian ?
Selandian - Mid Thanetian
U. T.
Selandian - mid Thanetian
NAB
SFA1S
SFA2
SFA3
DSP2
DSP1
SX
C0-C1
C2S
C2M
C2I
SC
SB
SA
C0
Int. C0'/C0
C1
Int. C1/C2
C2a
NP9
NP6-NP8
NP4-NP6
5 m
10 m
b
Eastern Gantour basin, sector Ben Guerir Nord
(Bout El Mezoud)
(well 88)
Ouled Abdoun basin
sector El Borouj (El Borouj)
sector Sidi Daoui (Recette IV)
sector Sidi Daoui (RP13-2)
sector Sidi Chennane Nord (P7)
NAB?
SFA1
SFA2
SFA3
DSP
C2S
C2I
C2a
C2b
C2b?
C3
C4
C5
C6
C7
SD
Int. C2/C3
45 m
2 m
Siliceous nodules
Chert
Phosphatic sands
Conglomerate
Phosphatic carbonates
Sandstone
Phosphatic calcareous sands
Yellowish clays
Phosphorites
Continental marls
Continental limestones
Phosphatic marls
Marine limestones
Marls
Danian to mid-Thanetian sediments
Maastrichtian sediments
Mining levels

Mining name	Sample	Depth (m) upper interval	Depth (m) lower interval	Interval thickness (m)	Depth (m) mean value
NAB	R620bis	12.50	12.90	0.40	12.70
NAB	R620	12.90	13.30	0.40	13.10
SFA1S	R6-18	15.80	16.50	0.70	16.15
SFA2S	R6-17	16.50	17.20	0.70	16.85
SFA2M	R6-16bis	17.20	17.60	0.40	17.40
SFA2M	R6-16	17.60	18.00	0.40	17.80
SFA2M	R6-15bis	18.00	18.40	0.40	18.20
SFA2M	R6-15	18.40	18.80	0.40	18.60
SA3S	R6-13	19.10	19.50	0.40	19.30
SA3S	R6-12	19.50	20.30	0.80	19.90
SFA3I	R611	20.30	21.00	0.70	20.65
DSP2	R6-8	22.70	23.40	0.70	23.05
DSP2	R6-78987	23.40	23.80	0.40	23.60
DSP1	R6-30	26.95	27.30	0.35	27.13
DSP1	R6-29	27.30	27.75	0.45	27.53
C0-C1	R6-28	27.75	27.90	0.15	27.83
SX	R6-79187	30.10	30.55	0.45	30.33
C2S	R6-27	31.60	32.00	0.40	31.80
C2S	R6-26	32.00	32.30	0.30	32.15
C2S	R6-25	32.30	32.70	0.40	32.50
C2S	R6-24	32.70	33.30	0.60	33.00
C2M	R6-79184 bis	33.70	34.15	0.45	33.93
C2M	R6-79184	34.15	34.60	0.45	34.38
C2M	R6-79183 bis	34.60	35.15	0.55	34.88
C2M	R6-79183	35.15	35.70	0.55	35.43

$\delta^{13}C_{org}$ (‰, VPDB)	TOC (wt.%)
-26.76	0.30
-26.79	0.67
-26.71	0.71
-27.31	0.96
-27.47	0.81
-27.57	1.04
-27.97	1.09
-27.95	1.07
-28.05	0.71
-28.08	0.99
-28.09	1.07
-28.38	0.35
-28.44	1.09
-28.50	1.50
-28.27	1.03
-27.93	1.25
-27.90	1.37
-27.58	0.31
-27.50	1.16
-27.26	1.11
-27.30	1.06
-27.01	0.64
-26.99	0.61
-27.05	0.38
-27.13	0.31

Highlights

- Datation of phosphate-bearing sequences from the Moroccan western Gantour basin
- $\partial^{13}C_{org}$ chemostratigraphy is an appropriate correlation tool
- The refined stratigraphy implies at least the presence of Danian, Selandian, and mid-Thanetian rocks
- Phosphate deposition over a ~8.5 Myr long time period